GROWTH AND CHARACTERIZATION OF $LuFe_2O_4$ THIN FILM BY PULSED LASER DEPOSITION

LIU JUN

M.Phil

THE HONG KONG POLYTECHNIC UNIVERSITY

2010

The Hong Kong Polytechnic University
Department of Applied Physics

Growth and Characterization of $LuFe_2O_4$ Thin Film by Pulsed Laser Deposition

Liu Jun

A thesis submitted in partial fulfillment of the requirements for the degree of Master of Philosophy

August 2009

CERTIFICATE OF ORIGINALITY

I hereby declare that this thesis is my own work and that, to the best of my knowledge and belief, it reproduces no material previously published or written, nor material that has been accepted for the award of any other degree or diploma, except where due acknowledgement has been made in the text.

_____(Signed)

_____LIU Jun_____(Name of student)

Abstract

Recently mixed valence material $LuFe_2O_4$ has attracted great interest for its multiferroic properties originated from its electronic ferroelectricity. Unlike conventional ferroelectric material with a pervoskite structure, where the ferroelectric is driven by ion shift, the ferroelectricity in $LuFe_2O_4$ is driven by the charge ordered state (CO) in the so-called Fe-O double triangle layers with mixed valence of Fe^{2+} : Fe^{3+} =1:1. Giant room temperature magnetodielectric and dielectric tunability under electric field have been reported, suggesting that $LuFe_2O_4$ is promising for novel multifunctional storage element. However, all the studies have been focused on $LuFe_2O_4$ single crystal or ceramic. In this thesis, the study of growth and characterization of $LuFe_2O_4$ thin films are carried out and the following results have been obtained.

$LuFe_2O_4$ thin films have been successively grown on sapphire substrates. Substrate temperature during deposition is found to be a critical condition (at least 750^oC) for the $LuFe_2O_4$ phase formation, while the higher the substrate temperature the better of the crystallization. Oxygen pressure during film deposition and annealing is critical to film's electrical and magnetic properties since optimized oxygen pressure is essential to realize the right ratio of Fe^{2+}: Fe^{3+}. It is also found that extra amount of Fe oxide in the target helps formation of $LuFe_2O_4$ films, however, impurity phase and

interfacial reactions are present in the films.

X-ray diffraction and transmission electron microscopy have been used to characterize the structure and crystallization of the $LuFe_2O_4$ films. Electrical properties of $LuFe_2O_4$ thin film have been studied by using HP 4294A and HP 4194B RF impedance analyzers with gold inter digital electrodes coated on $LuFe_2O_4$ films surface. Dielectric tunability under DC bias voltage has been found in $LuFe_2O_4$ films, and the result is comparable to that found in the bulk material. Electric field induced phase transition has been explored in the $LuFe_2O_4$ film, where higher electric field is needed to break the charge ordering in the $LuFe_2O_4$ film than bulk. Temperature-dependent phase transition has also been found both in dielectric and resistance measurements, where at charge ordered (CO) transition temperature $LuFe_2O_4$ film experiences insulator-to-metal transition due to the charge ordering breakdown.

Magnetic properties have also been studied by vibrating sample magnetometer (VSM), where anisotropic magnetic properties of the $LuFe_2O_4$ film are found. Magnetic and electrical coupling has also been found in dielectric measurement, where the dielectric tunability under DC bias voltage of the sample is suppressed by a small magnetic field.

List of publications

J. Liu and J.Y. Dai[+] "Structural and dielectric properties of $LuFe_2O_4$ thin films grown by pulsed-laser deposition" *Thin Solid Films, submitted.*

J. Liu, P.F. Lee, K.C. Chan, K. Zhang, Yu Wang and J.Y. Dai[+]
"Temperature-dependent resistance and magnetoelectric coupling in LuFe2O4 thin film deposited by pulsed-laser deposition" *Japanese Journal of Applied Physics*

Acknowledge

I would like to express my sincere gratitude to my supervisor Dr J.Y. Dai for his excellent guidance and invaluable advice throughout the whole period of my research study. Especially thanks for his consistently support, when the project be in a dilemma. I would also like to give my deep thanks to Prof H.L.W. Chan, Prof F.G. Shin, Prof K.H. Wong. Dr Y. Wang, Dr Y.W. Wong for their fruitful discussion and assistance on my research work and coursework studies.

I would also like to thank Dr. P.F. Lee, Miss. K.C. Chan, Mr. J.X. Zhang, Dr. W. Huang, Mr. Z.P. Wu, Dr. G.Y. Wang, Mr. J. Yong and Mr. K. Zhang for their help assistance and suggestion on my work.

I would like to thank Mr. M. N. Yeung of the Materials Research Centre for his assistance in the structure characterization.

I would like to give my thanks to my colleagues and friends in AP: Mr. H.K. Lau, Mr. W.K. Lee, Miss. H.L. Li, Miss, W.P. Suen, Mr. H.F. Wong. Mr. M.X. Chao and Mr. B. Guan for their help and discussion on my research work.

I gratefully acknowledge the financial support from the Department of Applied Physics and the Centre for Smart Materials of the Hong Kong Polytechnic University

Finally, I would like to express my deepest appreciations to my parents for their support, understanding and love through my undergraduate and postgraduate studies. Without you this would have been impossible.

Table of content

List of figures and tables

Chapter 1 Introduction

1.1 Multiferroic material and their properties

1.1.1 What is multiferroic?

Multiferroic materials have attracted extensively study recently, because of their interesting physics involved as well as promising properties for important practical applications such as multi-states memory elements, electric controlled ferromagnetic resonance devices, transducers with magnetically modulated piezoelectricity. However, much of the early work was based on the attempt of bringing ferroelectricity and magnetism together in one material, which started in 1960s, predominantly by two groups in Soviet Union: the group of Smolenskii [G.A. Smolenskii, 1971], and Venevtsev in Moscow [Y.N. Venevtsev, 1994]. Before an upsurge of these problems started from 2001-2003, this field of research had not received much attention. The upsurge of this research is due to three factors [D.I.Khomskii, 2008]. First, the development of techniques in preparing and studying thin films provides an opportunity to better study and use these ferroelectric materials. Second, many new multiferroic systems, such as $TbMn_2O_5$[N. Hur, 2004], $TbMnO_3$ [T. Kimura, 2003], $Ba_{0.5}Sr_{1.5}Zn_2Fe_{12}O_{22}$[T. Kimura, 2005], and $Ni_3V_2O_8$[G. Lawes,2005], with the coupling between ferroelectricity and magnetism, have been discovered since then. Third, a much broader realization of these novel materials and new technical facilities probably give ideas of very interesting and promising applications, such as multiferroic memory.

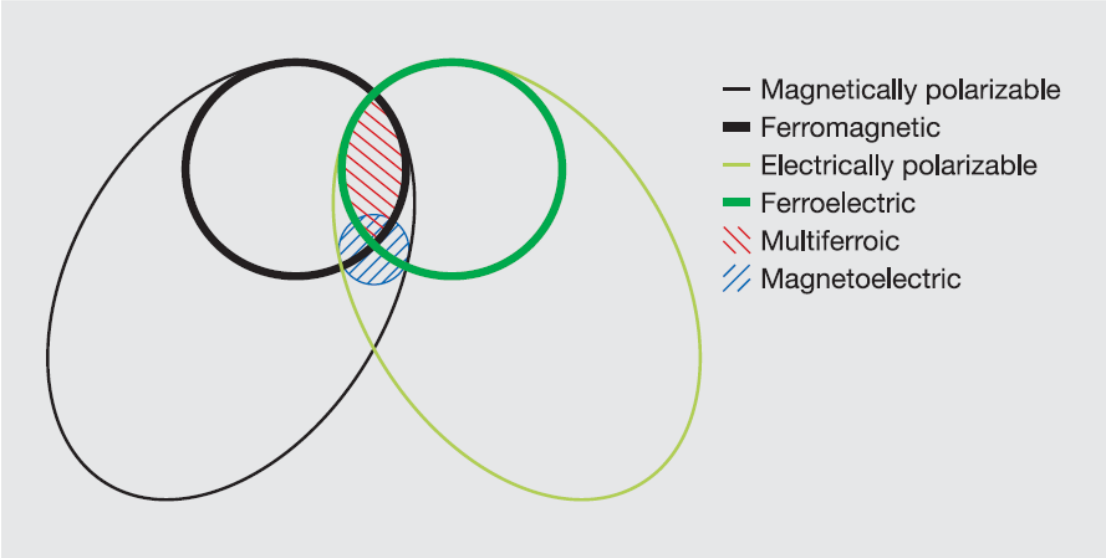

Fig.1.1 Schematic diagram showing relationships of multiferroics

This field of research has involved many terms, such as “multiferroic” and “magnetoelectrics”, whose overlap is ambiguous. The relationship is now explained in Fig.1.1 [W. Eerenstein, 2006]. From this figure, the area “multiferroic” is different from the area of “magnetoelectric”, which is the most applicable part in the multiferroic topic. The term “multiferroic” is originally defined as a kind of material that processes two or all three of the so called “ferroic” properties: ferroelectricity, ferromagnetism and ferroelasticity. However, the current trend is to exclude the requirement of ferroelasticity, but to include the ferrotoroidic order. Moreover, antiferroic order has been included to the classification of multiferroics. Magnetoelectric on the other hand, may exist whatever the nature of magnetic and electric order parameters are, and may arise directly between two order parameters, or indirect via strain[W. Eerenstein, 2006]

The first discovered multiferroic material is nickel iodine boracite, $Ni_3B_7O_{13}I$ [E. Ascher, 1966]. This material was followed by synthesis of many boracites compounds with complex structure and more than one formula unit per unit cell. The large

number of inter-ionic atoms in this kind of material gives rise of the isolation of the factors of the multiferroic and also prevention of the coupling between magnetic, electric polarization, and structure order parameter. After the resurgence of this field, several new multiferroic materials have been found and studied, which have different microscopic sources of ferroelectricity compared to traditional perovskite structured ferroelectric materials.

The current revolution in multiferroic material discovery is orthorhombic rare-earth manganites $RMnO_3$ (R is rare-earth material, such as Tb, Dy), whose electric dipole is probably induced by spiral magnetic ordering below 28 K.[M. Kenzelmann etc 2005] In $Tb(Dy)MnO_3$, high magnetic tunability of dielectric constant and electric polarization have been found. [T. Goto 2004] Under magnetic field, the spin-flip transition has occurred in the system and cause polarization rotated by 90^o and the dielectric constant increase ~500% in a narrow field range. However, the ferroelectricity only exits in a certain phase, and strong coupling has been demonstrated between magnetic and electric subsystems. These materials are hardly applicable due to their narrow working temperature range but are more interesting in theoretic studies of their mechanism.

$LuFe_2O_4$, another "improper" ferroelectric material, whose ferroelectricity is caused by the charge ordering of Fe^{2+} and Fe^{3+}, with average valence $Fe^{2.5+}$ (T_c = 320 K) in the bilayer structure, has drawn strong interest. The ferroelectricity in $LuFe_2O_4$ has been proved to be electronic ferroelectricity and demonstrated by pyroelectric current measurement with large polarization compared to other improper ferroelectrics. [N. Ikeda, et al., 2005] Giant magnetodielectric property at room temperature has been recently found in this material [M. A. Subramanian 2006], in which the dielectric constant shows very high tunability by small magnetic field of ~0.2 T. Although the origin of the coupling between the magnetic and electric

subsystems is not fully understood, the multiferroic properties are thought to be related to charge order state transition. [H. J. Xiang 2007]

1.1.2 The discovery of coexist of ferroelectricity and ferromagnetism

In 1865, James Clerk Maxwell proposed the four equations, named after him, governing the dynamics of electric fields, magnetic fields and electric charges [J. C. Maxwell, 1865]. The four equations show the intrinsic coupling between magnetic interactions and motion of electric charges which were initially thought to be two independent phenomena. The unified nature of magnetism and electricity are succinctly reflected in the covariant relativistic form of Maxwell's equations when they reduce to just two equations for the electromagnetic field tensor [L. D. Landau, 1962]. A number of interesting parallels exist between electric and magnetic phenomena have been discovered in twentieth century, such as the quantum scattering of charge off magnetic flux (Aharonov–Bohm effect [Y. Aharonov, 1958]) and the scattering of magnetic dipoles off a charged wire (Aharonov–Casher effect [Y. Aharonov, 1984]).The numerous similarities in the thermodynamics of ferroelectrics and ferromagnetics, explained by formal equivalence of the equations of electrostatics and magnetostatics in polarizable media, are particularly striking in the initial view of the seemingly different origins of ferroelectricity and magnetism in solids: whereas magnetism is induced by ordering of spins of electrons in incomplete ionic shells, for example Fe_3O_4; while ferroelectricity results from relative shifts of negative and positive ions that induce surface charges, like $BaTiO_3$. The pioneering discovery shows that though the ferroelectricity and ferromagnetism can arise independently in a single-phase material, but they are rare [W. Eerenstein, 2006]

Hill explained why there are so few materials with ferroelectricity and

ferromagnetism coexistence in her paper in 2000[Hill 2000]. The most traditional ferroelectric materials are transition metal oxides, in which the empty *d* shell in transition metal is favorable to attract neighboring negative oxygen ions. The position shifts of cations and anions in periodic lattice structure cause electric polarization in material. On the contrary, magnetism requires partially filled *d* shell in transition metal ions, as the spins of electrons in the fully filled shell are added up to zero and do not contribute in magnetic ordering. The spins exchange in uncompensated shell of different ions give rise to a long range magnetic ordering, such as $BiMnO_3$ and $BiFeO_3$. [Seshadri, R. 2001] Although the mechanisms of them are not dissimilar, the difference in filling requirement of *d* shell for ferroelectricity and ferromagnetism causes mutual exclusive between them. [Hill, 2000]

Those ferroelectrics, associated with electronic pairing in traditional perovskite material, induced by structural instability to the polar states, is called ‘proper’ ferroelectrics. However, if the electric polarization is induced only from a part of some kind of more complex lattice distortion or if it is occurred as an accidental by-product from some other ordering, like magnetic ordering in $RMnO_3$ [M. Mostovoy, 2006 & M. Kenzelmann, 2005] and charge ordering in $LuFe_2O_4$, the ferroelectricity is called ‘improper’ [A.P. Levanyuk, 1974]. Although both ferroelectric and ferromagnetism may be strong in ‘proper’ ferroelectric material, like $BiMnO_3$ [T. Kimura, 2003], their coupling is weak, because those properties are associated with different ions. Comparing to ‘proper’ ferroelectric, the restriction of coexistence with ferromagnetism is however low in ‘improper’ ferroelectric material. In fact, materials with magnetic ordering induced electric dipoles are one of the best candidates for useful multiferroics [S.W. Cheong, 2007], because such electric polarizations are highly tunable with applied magnetic fields.

Compared to those extensively studied ferroelectric coupling with magnetic

frustrated system, the charge ordering induced ferroelectric, such as $LuFe_2O_4$ is new comer to expand this field, and the mechanism of multiferroic coupling in this material are not well understood, and still being discussed [N. Ikeda, 2005a; M. A. Subramanian, 2006; H. J. Xiang, 2007; A.D. Christianson, 2008]. Compared to frustrated 'geometric ferroelectrics', electronic ferroelectric have larger polarization [N. Ikeda, 2005a] and wider working temperature range [M. A. Subramanian, 2006], therefore attracted more and more attention recently.

1.2 Structure and property of lutetium iron oxide ($LuFe_2O_4$) system-Introduction to $LuFe_2O_4$

$LuFe_2O_4$ belongs to RFe_2O_4 family, in which R is rare earth material from Dy to Lu and Y. RFe_2O_4 family is compounds having a rhombohedral structure with space group $R\bar{3}m$. Its crystal structure consisting of alternating stacks of mixed valence Fe and rare earth oxide triangular lattice is shown in Fig 1.2 in hexagonal form (a=3.438Å and c=25.25Å for R=Lu).[N. Kimizuka, 1990] An equal amount of Fe^{2+} and Fe^{3+} are in the same site of the triangular iron plane with average valence $Fe^{2.5+}$. The interaction between Fe^{2+} and Fe^{3+} is accomplished as a frustrated system in triangle plane, which is essential to both electrical and magnetic properties to RFe_2O_4 family.

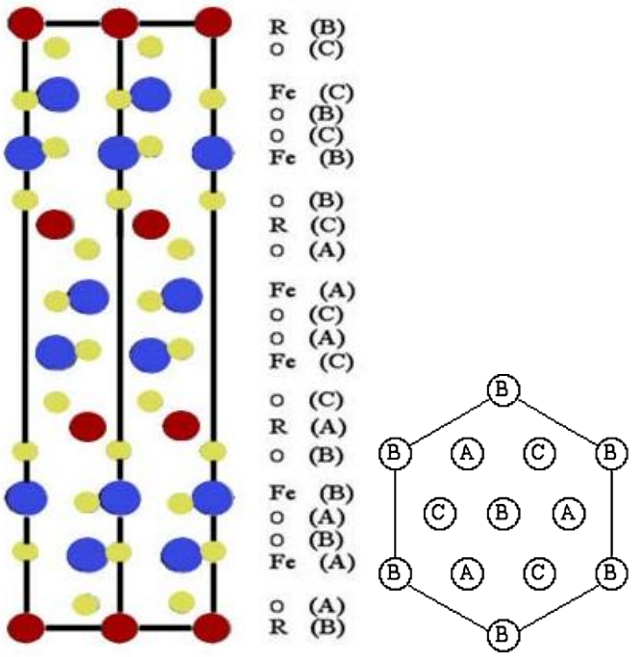

Fig.1.2 Crystal structure of RFe_2O_4 compound with stacking Fe and rare earth triangular planes. The positions of A, B, C on hexagonal plane are also shown on the right. [M. Isobe, 1990]

$LuFe_2O_4$ was first proved to be a ferroelectric material in 2005 by N. Ikeda.[N. Ikeda,2005a] The macroscopic electric polarization was deduced from pyroelectric current measurement, as shown in Fig. 1.3, in which the sign of current changes by applying electric field in different directions. Moreover, in this experimental result, an observable current drop was found at 250 K, the Neel temperature of this material, indicating a coupling between magnetism and electric polarization. This experiment is a milestone in the $LuFe_2O_4$ research attracting more attention to this material since then.

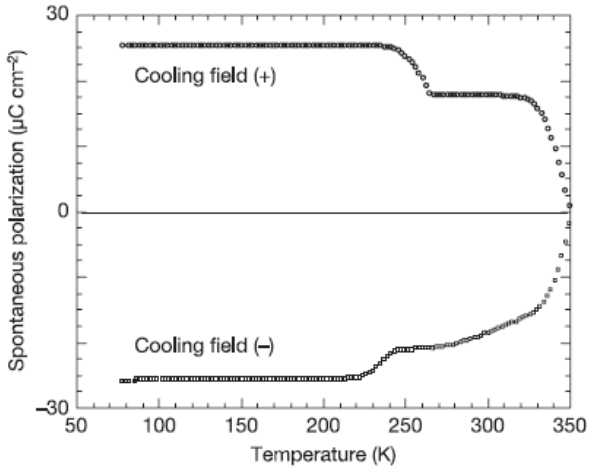

Fig.1.3 Polarization as a function of temperature from $LuFe_2O_4$ single crystal by pyroelectric measurement. [N. Ikeda, 2005]

Some more reports revealed more multiferroic properties of $LuFe_2O_4$, and therefore confirmed $LuFe_2O_4$ as a multiferroic material. Magnetodielectric effect was found by M.A. Subramanian, as shown in Fig.1.4, in which 20% more change in dielectric constant can be seen with an applied magnetic field of 0.2 T which is a very small external magnetic field.

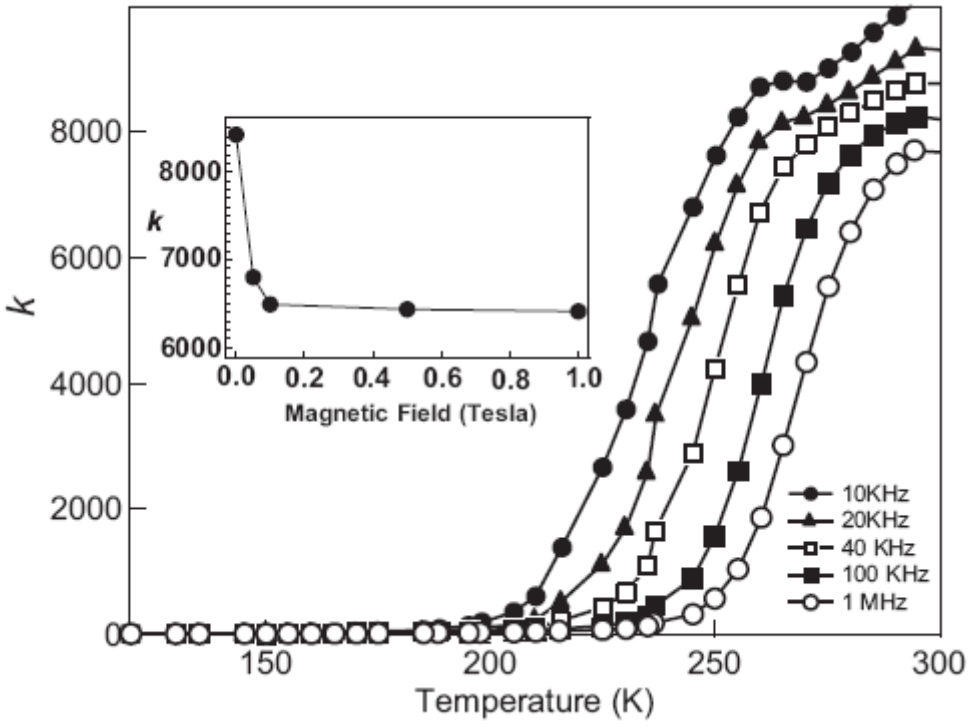

Fig.1.4 Temperature-dependent dielectric measurement from 70 to 300 K, with the inset diagram showing the magnetodielectric effect under external magnetic field. [M. A. Subramanian, 2006]

Electric field induced magnetization was also realized in $LuFe_2O_4$ single crystal [C.H. Li, 2009] as shown in Fig.1.5, where a reversible magnetization cycle is induced by both electric and magnetic fields. A critical voltage of 22 V was applied to the a-b plane and magnetic field was applied to the c-axis, the easy axis of $LuFe_2O_4$. In this measurement, the magnetization can be switched up at 200 K temperature under 0 T and switched down under 0.1 T magnetic field, but the switching is independent of the direction of voltage applied. The author explained the mechanism as that the magnetization states were changed by charge-ordered states breakdown induced by electric field and local heating, and conduction filament was not the appropriate reasons. The physical process is explained in this way: a charge ordering melting (also known as charge ordering breakdown) causes releasing of localized charge carriers, therefore induces a magnetization excitement where the energy state is changed through a magnetoelectric effect. This is said: the change in electric state of electrons changes the magnetization of the material.[C.H. Li, 2009]

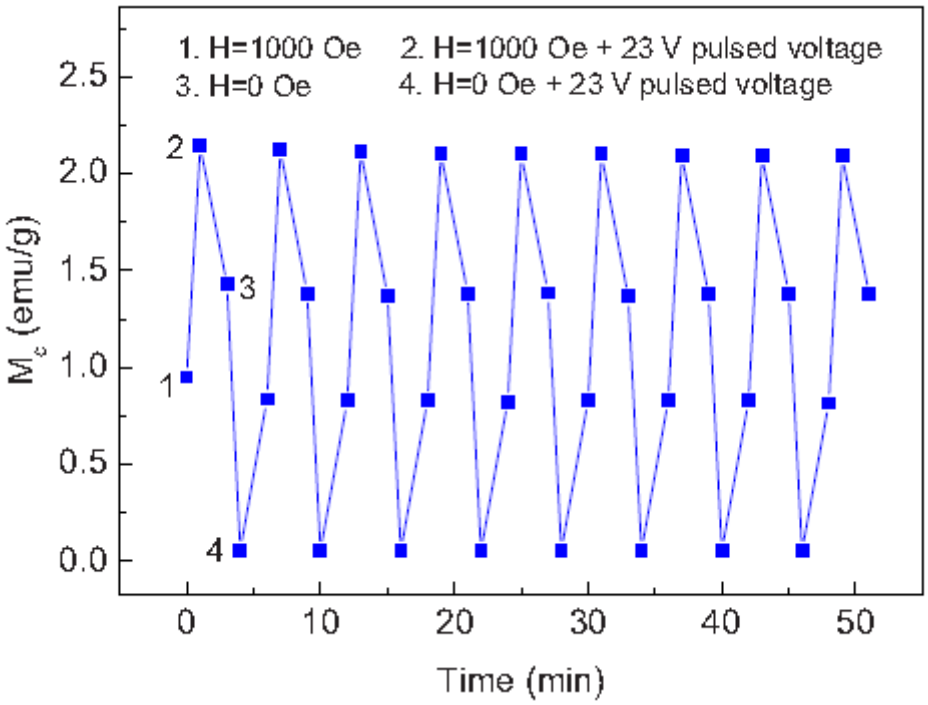

Fig.1.5 Reversible magnetization switching at 200 K

Two more properties related to charge order breakdown are dielectric tunability by DC bias voltage [C.H. Li, 2008 a] and insulator-to-metal phase transition under electrical field [C.H. Li, 2008 b]. Dielectric tunability is a common feature in ferroelectric materials [K. M. Johnson, 1962; A. Feteira, 2004]. The dielectric tunability of more than 50% was recently reported in $LuFe_2O_4$ ceramics [C.H. Li, 2008 a], as shown in Fig.1.6, in which a polarization suppression is caused by CO break down which is different from conventional ferroelectric material. The electric field (50V/cm) required for dielectric tunability in $LuFe_2O_4$ is several orders of magnitude lower than that of other materials (normally in order of kV/cm). Although $LuFe_2O_4$ is insulating material at room temperature, the dielectric loss is relatively high (0.2-0.5 and increases with dc bias voltage) at low frequency as show in Fig.1.7 (b), which is a drawback for $LuFe_2O_4$ as a candidate for application of tunable electronic device.

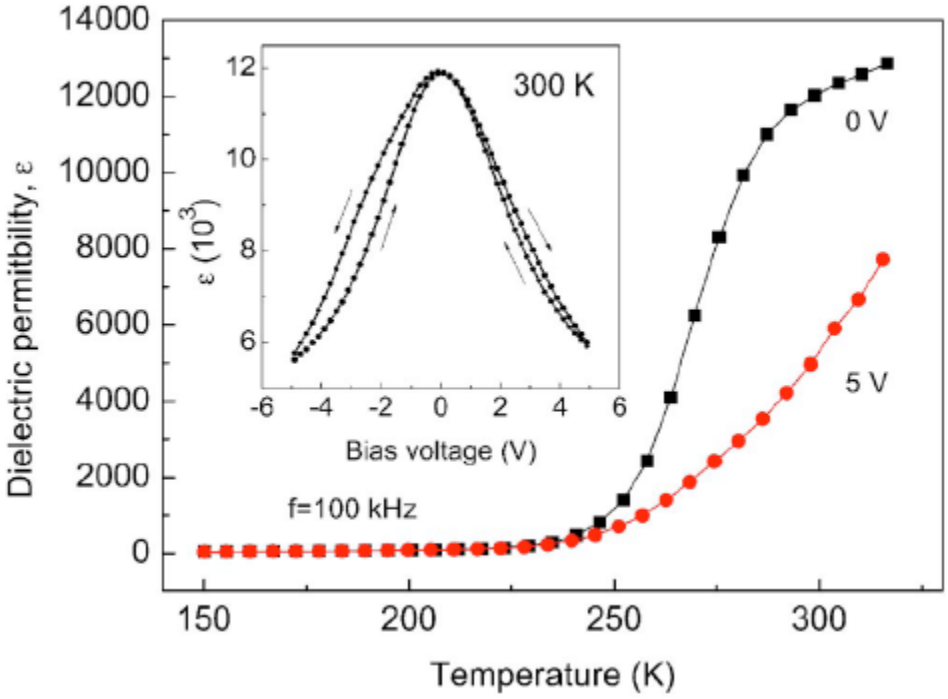

Fig.1.6 DC bias voltage influenced dielectric tunability in $LuFe_2O_4$ measured at 100 kHz, where the inset diagram is the permittivity change with bias voltage increase. [C. H. Li, 2008a]

The insulator-to-metal phase transition was also investigated by *Li et al* recently in $LuFe_2O_4$ [C.H. Li, 2008 b], in which CO states breakdown was observed by resistance measurement. As shown in Fig. 1.7, resistance measurement was performed at different temperatures from 240 to 340 K with increased voltage to explore the relation between the electric field and temperature induced insulator-to-metal transition. The experimental results reveal that, as temperature increases, the electric field required for CO melting decreases. This phenomenon was also explored in classical lodestone Fe_3O_4, and CO melting trigged by electrical field was also believed to be the reason. These experimental results suggest that charge-ordered state plays an essential role in electrical properties of $LuFe_2O_4$. Several theoretic investigations have been made to approach the CO modes in $LuFe_2O_4$ to explain the mechanism behind all these phenomena mentioned in this chapter. The recent discovery in theoretical

work will be discussed in session 1.2.2. Although, the complexity of the CO state in this material is like Fe_3O_4, it is still not fully understood due to the lack of efficient methods to reveal the charge ordered structure in the material.

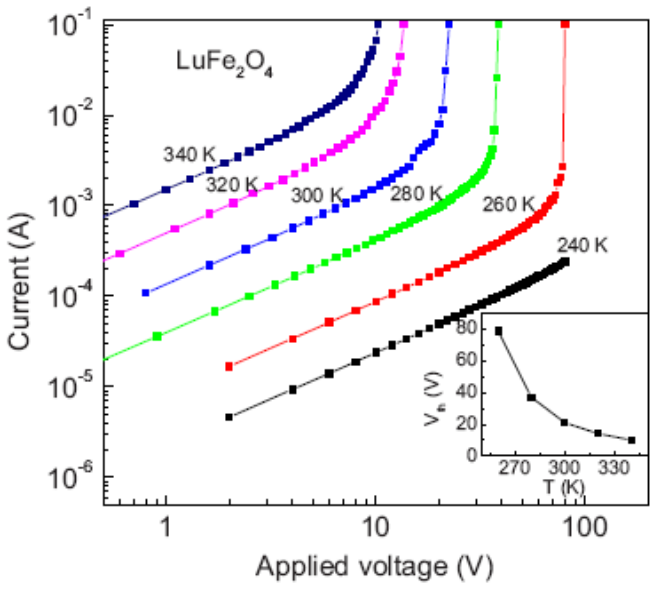

Fig.1.7 Voltage-induced phase transition measured at different temperatures. The inset diagram shows that the voltage required to cause the phase change decreases as temperature increases. [C. H. Li 2008 b]

1.2.2 Charge-ordered states in $LuFe_2O_4$ system

A charge-ordered state transition in $LuFe_2O_4$ from three dimensional (3D) to two dimensional (2D) is at 330 K, and from 2D to disordered state is at 500 K. Charge-ordered states were considered as an essential factor behind various behaviors of $LuFe_2O_4$, including pyroelectric current [N.Ikeda, 2005], magnetodielectric [M.A. Subramanian, 2006], electric field induced magnetization [C.H. Li, 2009], dielectric tunability [C.H. Li, 2008 a] and insulator-to-metal transitions[C.H. Li, 2008 b]. For example, the charge-ordered state transition temperature from 3D to 2D is as same as the Curie temperature of $LuFe_2O_4$, indicating a strong relation between ferroelectric essential with charge-ordered states in $LuFe_2O_4$.

However, the explanation of charge-ordered state is not fully built up yet. A postulate mode of Fe^{2+} and Fe^{3+} superstructure in adjacent triangle layers has been proposed in early work [N. Kimizuka, 1990], in which the centers of Fe^{2+} and Fe^{3+} do not coincide, resulting in a local electrical polarization in it (Fig.1.8). Ikeda had made an improvement to this model with theoretic postulate model of 36 possible configurations in anti-ferroic order and with resonant X-ray scattering (RXS) experiment proved that the polarization is induced from Fe^{2+} and Fe^{3+} in $LuFe_2O_4$.

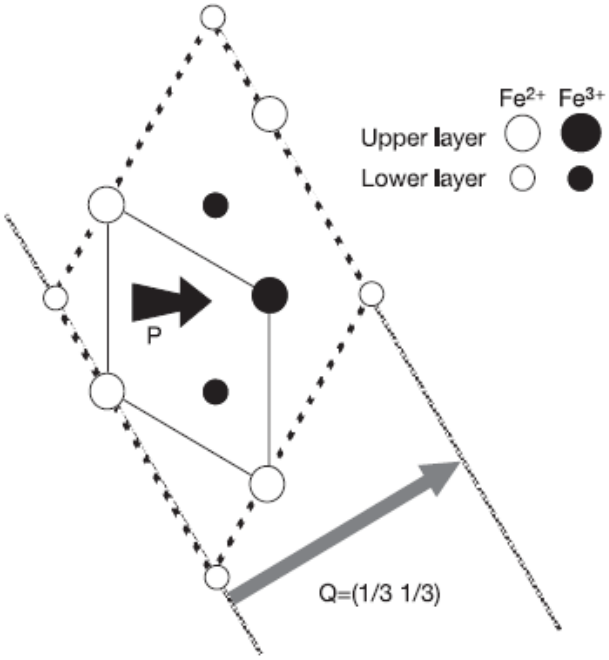

Fig.1.8 Model of the charge ordering in adjacent triangle layers. Solid line is the chemical unit cell. The dotted line is the charge $\sqrt{3} * \sqrt{3}$ super cell. Large and small circles represent the Fe ion in upper and lower layers, respectively. White and black circles represent Fe^{2+} and Fe^{3+}, respectively. The polarization ***P*** is represented with a short black arrow. The long grey arrow represents the wave vector Q. [N.Ikeda, 2005b]

However the CO models above didn't give rise to macroscopic polarization, which cannot explain the experimental result of pyroelectric current measurement. A

possible charge-ordered state related to this phenomenon was proposed by H. J. Xiang *et al*, a group in North Carolina State. [H. J. Xiang, 2007] The model was built by first-principle electronic structure calculation and Monte Carlo simulation of electrostatic energy, in which two types CO states in ferroelectric order were given out to be the possible states in $LuFe_2O_4$ at room temperature. These two CO states have very closed energy levels, only 20 meV/f.u. difference, at room temperature, but with different polarizations. The theoretical value of $LuFe_2O_4$ electric polarization is 26.3 $\mu C/cm^2$ in this CO states model, which perfectly matches the experimental result in Ikeda's work which is 25 $\mu C/cm^2$. [N. Ikeda, 2005a] However, the model given by H. J. Xiang at first purpose was to give an origin of the giant magnetodielectric effect in $LuFe_2O_4$ [M.A. Subramanian, 2006]. Under external magnetic field, these two CO states, with close energy states, will converge to one, therefore reduces polarization switch in dielectric measurement. Still, the model cannot fully explain the CO states behavior, as it cannot demonstrate how magnetic field works with the CO states switching.

Other than the Resonant X-ray Scattering (RXS) experimental demonstration on the charge ordering in $LuFe_2O_4$, more experiments were carried out on it. Direct observation of charge ordering from transmission electron microscopy (TEM) has been reported in 2007. [Y. Zhang 2007] The TEM result taken at temperature of 20 K is shown in Fig.1.9 (a), in which the stripe between the main spots is illustrated in Fig.1.9 (c), where q_1 modulation was thought to be the superstructure of charge ordering from Fe^{2+} and Fe^{3+}. Y. Zhang suggested that the ferroelectric charge ordering ground state was realized by this charge stripe ordering at low temperature. According to the rhombohedral symmetric in $LuFe_2O_4$, a spontaneous polarization in c-axis direction will be generated, therefore results in electronic ferroelectricity in $LuFe_2O_4$.

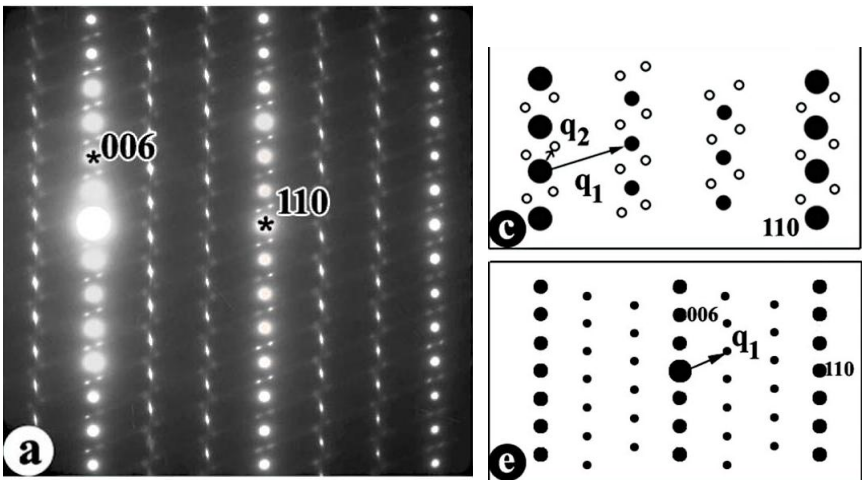

Fig.1.9 (a) Diffraction pattern of $LuFe_2O_4$ single crystal along [110] direction, (b) and (c) proposed charge ordering mode . [Y. Zhang, 2007]

1.2.3 Magnetic correlation in $LuFe_2O_4$

In $LuFe_2O_4$, two dimensional ferromagnetic spin ordering has been investigated by neutron scattering studies below 240 K and the easy axis of $LuFe_2O_4$ is c-axis [J. Iida 1990]; while above 240, paramagnetic phase appears. The spin structure is suggested by Mössbauer spectroscopy measurement [M. Tanaka 1989], in which both Fe^{2+} and Fe^{3+} are classified as three groups. The experimental result indicates that there are 1/3 Fe^{3+} spins aligned parallel to the external magnetic field; while 2/3 Fe^{3+} spins are placed in the opposite direction to the external magnetic field; and all the Fe^{2+} spins are parallel to the direction of external field. The postulated spin arrangement model was proposed by Siratori *et al* and is shown in Fig.1.10 [K. Siratori 1992]. In this model, a primary importance can be revealed on the antiferromagnetic coupling between Fe^{3+} - Fe^{3+}, in which the lowest energy state can be realized at the cost of Fe^{2+} - Fe^{2+} and Fe^{2+} - Fe^{3+}.

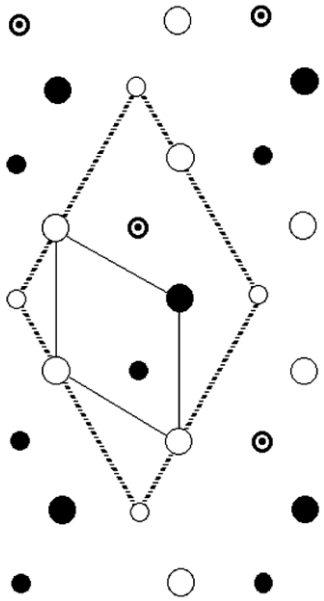

Fig. 1.10 Spin arrangements in super lattice proposed by K. Siratori, [K. Siratori 1992]

However, recently, *Christianson et al*, a group in USA, demonstrated three dimensional correlated spin ordering in $LuFe_2O_4$ below 240 K and found an additional magnetic transition temperature at 175 K based on neutron scattering results [A.D. Christianson, 2008]. This difference is probably due to the physical property of RFe_2O_4 family that strongly depends on oxygen stoichiometry, and therefore highly depends on sample's quality, which has been reported in experimental work [S. Funahashi,1984]. Below T_N new intensity appears at integer L as neutron diffraction scanning along (1/3 1/3 L), providing an evidence for 3D magnetic correlation in $LuFe_2O_4$. The two transition temperatures are clearly shown in Fig.1.11, in which the integrated intensity is plotted against temperature for the magnetic peak at (1/3 1/3 0), and the low temperature magnetic transition is also confirmed from cooling curve of magnetization along c-axis.

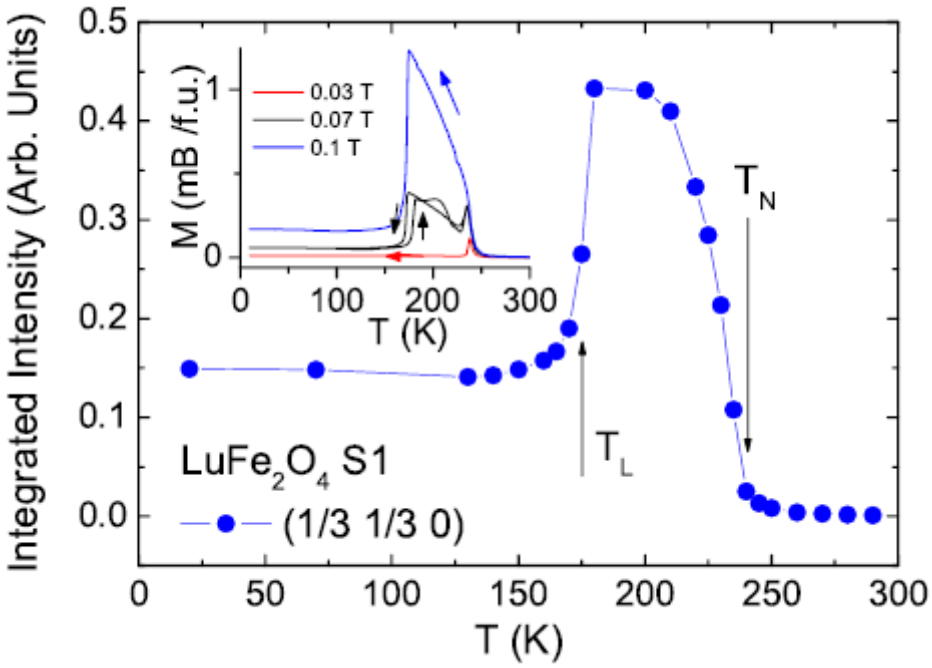

Fig.1.11 Integrated intensity at (1/3 1/3 0) plotted against temperature with inset diagram of field cooling along c-axis magnetization data. [A.D. Christianson, 2008]

Various methods have been used to investigate the magnetic ordering in $LuFe_2O_4$, including neutron scattering [M. Kishi, 1982], vibrating sample magnetometer[B. K. Bang, 2008], resonant x-ray diffraction [A. M. Mulders, 2009], and Fe Mössbauer spectroscopy [M. Tanaka, 1989 & 1993]. Theoretical studies have also been carried out to reveal the spin ordering in $LuFe_2O_4$, such as local density functional calculation by Monte Carlo method.[H. J. Xiang, 2008] Spin ordering investigation provides a alternative way to understand the mechanism of multiferroic properties of $LuFe_2O_4$, as now there is no sufficient method to investigate the charge ordering state structure in a material.

1.2.4 Motivation of this project

The relentless demand on higher performance in modern technology always drives scientists to find novel materials. The broader realization of novel materials can also help to think of many interesting and very promising applications. Multiferroic materials have attracted extensively investigation since 2000 [N.A Hill 2000] due to the prospect of controlling charges by applying magnetic field or controlling spins by applying electric field, leading to the invention of new generation devices. Due to the exclusive mechanism in ferroelectric and ferromagnetism, a new type of ferroelectric material, so called improper ferroelectrics [Levanyuk 1974], has been intensely studied to extent the limited range in multiferroic materials, for instance, magnetic ferroelectric $TbMnO_3$ [Kenzelmann 2005] and electronic ferroelectric $LuFe_2O_4$ [N. Ikeda 2005].

$LuFe_2O_4$, among those new multiferroics, is particularly interesting due to the following reasons. First, the dielectric properties are interesting, for instance, it has dielectric tunability, and its magnetodielectric can exist in room temperature. Magnetodielectric has been found in $BaMnF_4$ [D. L. Fox 1980], $GdAlO_4$ [M. Mercier 1970], $DyPO_4$ [G. T. Rado 1969], $GdVO_4$ [G. Gorodetsky 1973], $BiMnO_3$ [T. Kimura 2003] and $YMnO_3$ [Z. J. Huang 1997] around their magnetic phase transition temperatures which are normally very low, for instant 100 K for $BiMnO_3$, to show large magnetodielectric property. None of them have been observed with significant change in dielectric constant at or above room temperature. Therefore, $LuFe_2O_4$ shows its spectacular property not restricted to magnetic transition temperature. Second, charge-ordered state makes several possible phases in $LuFe_2O_4$ [N Ikeda 2005b] which are essential to most physical properties. For example, resistance [Changhui Li, 2008], dielectric constant [Changhui Li,2008b; M. A. Subramanian 2006], electric polarization[N Ikeda 2005; N. Ikeda 2005b], magnetization [Changhui Li, 2009] etc, are found to be changed with either electric field, magnetic field or temperature. Although, the detail of phase transition is not completely understood,

possible explanation has been proposed by showing Fe^{2+} and Fe^{3+} arrangement which contributes to both magnetic and electric ordering [N Ikeda 2005b]. This essential property promises a significant potential to application, for it provides an extra degree of freedom in control. For example, the dielectric constant decrease was found both under magnetic field [M. A. Subramanian 2006] and electric field [Changhui Li,2008b]. Third, comparing to other improper ferroelectrics, such as $TbMnO_3$ [Kimura. T, 2003] with a polarization of 0.08 $\mu C/cm^2$, $LuFe_2O_4$ has a large ferroelectric (FE) polarization (25 $\mu C/cm^2$ under 250 K, 17 $\mu C/cm^2$ under 340 K) [N. Ikeda 2005] and a large dielectric constant (in the order of 10^4) [K. Yoshii, 2007], therefore, those properties in $LuFe_2O_4$ are easier to be measured and more suitable for practical applications. Forth, electrically induced magnetization switching, the reversal ME effect, is usually rare to be observed, but recently has been successfully realized in $LuFe_2O_4$ single crystal [C.H. Li 2009].

Physical properties of $LuFe_2O_4$ have been intensely studied in single crystal [Y. Zhang, 2007; A. M. Mulders, 2009; Y. L. Ma, 2009] and ceramic forms [C. H. Li, 2008]. However, there is no reported on $LuFe_2O_4$ thin film so far. One reason is that its multiferroic properties were not fully explored until recently and another reason is that most research work has been focused on its physical phenomena, such as charge and spin ordering coupling. By fabricating thin film in different substrates, it can provide desired orientations of high quality films in application of integrate electronic devices. Furthermore, single phase oxide films have been proved to introduce novel properties [W. Prellier, 2005] because of strain induced structural transition. For example, $BiFeO_3$ is rhombohedral in bulk form, but has been successfully transformed to monoclinic structure on (100) $SrTiO_3$ substrate [Wang 2003] and tetragonal structure on Si substrate [Yun 2004]. The enhanced spontaneous polarization was observed by Wang *et al* in $BiFeO_3$ thin film (increases from 6.1 $\mu C/cm^2$ to 50–60 $\mu C/cm^2$, almost an order of magnitude higher). These results confirm that stress in the

film strongly influences the ferroelectric properties of $BiFeO_3$, and such phenomenon in the case of oxides thin film is common and has already been reported. In manganites [Prellier W 2001], these effects have also been observed. Ferroelectric transition temperature can also be influenced by lattice distortion, and therefore can be varied from its original value when the material changes from bulk to thin film. The stress induced lattice distortion in thin film may unravel more physical phenomena, therefore improves the understanding of the ferroelectric mechanism.

In addition, the previous studies have observed high dielectric constant and its dispersion in $LuFe_2O_4$ bulk, which is a direct consequence of domain boundary effects. As a result, a much larger coupling is possible to engineer this material in thin film growth that may provide a much higher density of domains. Finally, the realization of thin film form $LuFe_2O_4$ is essential for this material to be used in integrated electronic devices.

1.3 Thesis organization

This thesis will be divided into five chapters:

Chapter 1 consists of introduction to the development in multiferroic materials and $LuFe_2O_4$, and motivation of studying $LuFe_2O_4$ thin film growth.

Experimental techniques used in this work and some of the background knowledge will be presented in *Chapter 2*.

Chapter 3 is the first chapter to present the experimental results of $LuFe_2O_4$ thin film growth and structural characterization. This chapter mainly deals with the experimental results and discussion of $LuFe_2O_4$ thin film structure, including

interfacial reaction and impurity phases.

Characterization of electrical and magnetic properties of $LuFe_2O_4$ film will be discussed in *Chapter 4*. Dielectric tunability and electric field induced phase transition is illustrated.

Finally, conclusions and suggestions for future work will be presented in *Chapter 5.*

Chapter 2 Experimental Technique and Background knowledge

The growth and characterization of $LuFe_2O_4$ films involve a number of advanced techniques and facilities. In this chapter, details of pulsed-laser deposition method for the film growth are introduced. Meanwhile structural characterization techniques including transmission electronic microscopy and x-ray diffraction are described. Electrical and magnetic characterizations and electrode structure for thin film measurements are also introduced.

2.1 Pulsed-laser deposition technique

In this project, to realize epitaxial growth of $LuFe_2O_4$ film is essential. There are variety of methods for thin film growth, among them pulsed-laser deposition (PLD) method provides a good way to fabricate high-quality oxide films. PLD provides a simple approach to transfer multiple compositions from target to substrate and a variety of ways to control the quality of films. [D. P. Norton, 2007]

Laser molecular beam epitaxy (LMBE) is a technique that combines the advantages of both PLD and MBE. Molecular beam epitaxy (MBE) is an important technology that enables atomic control and characterization of thin film growth process.

With a slow rate of deposition in high or ultrahigh vacuum, this important aspect makes MBE a promising technique for epitaxial thin film growth. PLD is a kind of physical vapor deposition to evaporate a large variety of metals or metal oxides or even multi-component targets with pulsed laser. PLD has been proven to be one of the most effective ways in growing crystalline oxides. The advantage of PLD exits in deliver of a growth flux with the relatively same stoichiometry to the target in an ambient with favorable oxygen pressure to control the desired phase in films [K. S. Sree Harsha, 2006]. Some researchers have attempted to combine MBE and PLD deposition technology base on their advantages. In 1983, a solid target was used by J. H. Cheung et al. in a traditional MBE system [J. H. Cheung, 1983]. In 1991, M. Kanai et al. attempted to use laser ablation method for the thin film growth under molecular beam epitaxy equipment condition [M. Kanai, 1991]. After these attempts, a new powerful technology has been initiated for preparing thin film materials.

A diagram of LMBE system is shown in Fig.2.1 consisting of a ultrahigh vacuum (UHV) chamber with connections to pre-load chamber, reflection high energy electron diffraction (RHEED) system, rotating target and substrate holder and a series of pumps including molecular pump, rotary pump and ion pump to obtain ultrahigh vacuum in the chamber.

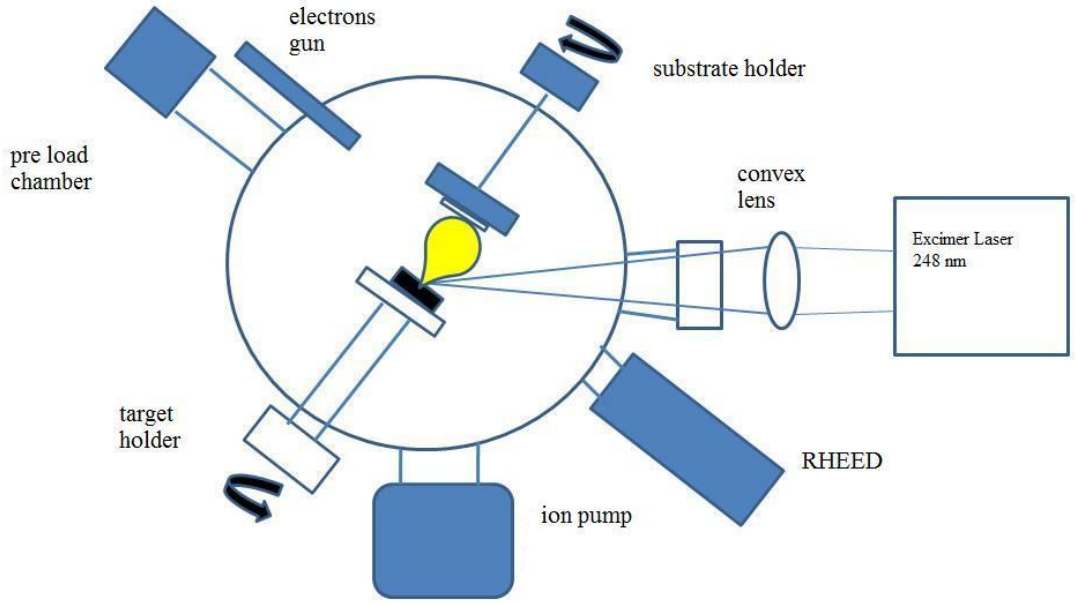

Fig.2.1 Schematic diagram of a LMBE system

In a PLD process, A KrF excimer laser with a wavelength of 248 nm and pulse duration of 25 ns (Lambda Physik COMPex 205) is focused on a ceramic target through a window in the chamber by a focus lens outside the chamber. When the laser energy density is above a threshold value, each laser pulse ablates a small amount of material from target creating a plasma plume. The physical phenomenon of the laser ablation and plume creation is quite complicated---the laser energy first converts to electronic excitation and then becomes chemical and mechanical energies, resulting in evaporation, ablation or plasma formation. For yielding epitaxial films, the ablation condition is chosen, normally laser energy and pulse frequency, such that the plume

primarily consists atomic, diatomic, and other low-mass species. The ejected species expand from the target with a strongly forward-directed trajectory toward a heating substrate placed in the line of the plume followed by the nucleation process and growth of crystalline films.

Base on the microstructure formed, the gown films can be categorized into three different types: epitaxy, polycrystalline and amorphous. The term epitaxy refers to monocrystalline film growing on monocrystalline substrate with a fixed orientation relation between film and substrate. The term polycrystalline refers to a film with randomly oriented grains. The term amorphous refers to a film without long range order, so no crystallization and grain can be observed. The nucleation process is normally described in three modes shown in Fig.2.2. [G. K. Hubler, 1994; M. Ohring, 1991; L.-C. Chen, 1994]:

1. Frank-van der Merwe, layer-by-layer growth mode. The total surface energy of the film surface and interface between film and substrate surface is lower than the surface energy of the bare substrate. In contrast to island growth mode, strong bonding is formed between film and substrate.

2. Stranski-Krastinov, layer plus island growth. In heteroepitaxial growth, lattice mismatch in interface gives rise to elastic strain inside the film, resulting in elastic energy with increased film thickness, and this growth mode occurred.

3. Volmer-Weber, 3-D island growth mode. Strong bonding is formed between the

atoms in deposited film, and there is no bonding between film and substrate.

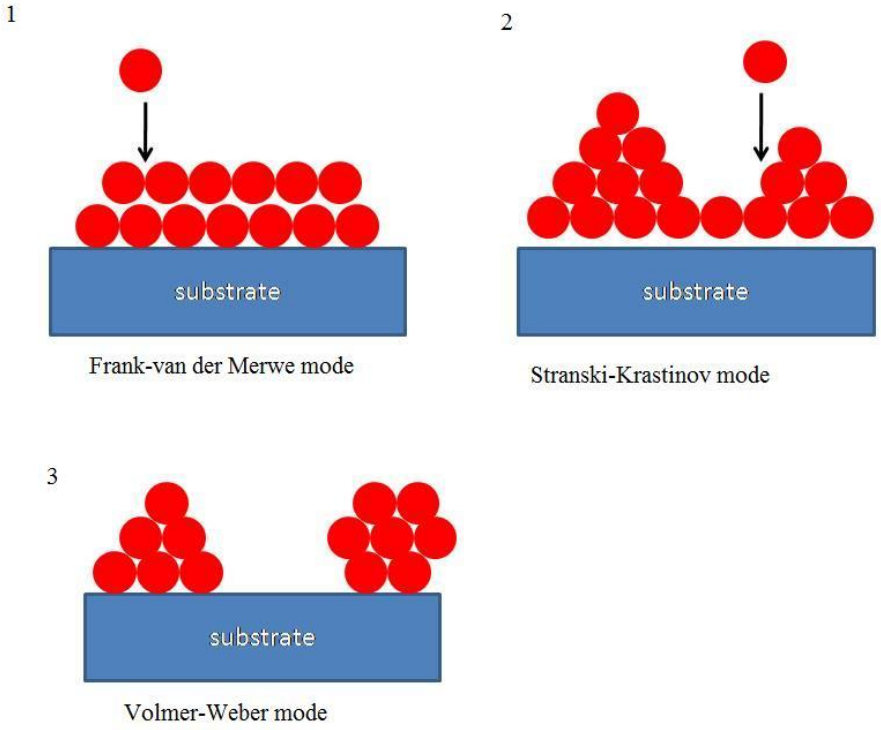

Fig.2.2 Film growth modes:(1) layer by layer (Frank-Van der Merwe), (2) mixed (Stranki-Krastanov), and (3) island (Volmer-Weber).

There are some other parameters affecting the film growth, such as target-to-substrate distance, ambient gas pressure and substrate temperature. The influence of target-to-substrate distance mainly affects the angular spread of ejected material flux in vacuum. However, in a poor vacuum, or in an ambient gas, or at a relatively large target-to-substrate distance, the ejected particulates may coalesce, depending on the position of the substrate [M. G. Norton, 1990]. An ambient gas is primarily used to compensate the loss of constituent element, for instance oxygen and nitrogen, in deposition process. Thus, by controlling the pressure of ambient gas,

epitaxial growth of thin film can be realized. The substrate temperature can influence the adhesion of the film and substrate and affect the surface mobility of the adatoms. [S. Metev, 1994] There also exits a critical substrate temperature, below which the crystallization of the film is incomplete and the stoichiometric composition ratio in the film is deviated significantly. [H. Hanafi, 1996]

2.2 Structural characterization

In this section, characterization methods will generally be described for both imaging (microscopy) and composition analysis (spectroscopy). The characterization techniques employed for the investigation of crystal structure and growth process will be discussed in the subsequent sections of this chapter.

The microstructure and interfacial structure of the $LuFe_2O_4$ films were investigated by high-resolution transmission electron microscopy (HRTEM) using JEOL 2010 electron microscope equipped with energy dispersive X-ray (EDX) analysis. The crystallization and the orientation of grains in the film were investigated by Bruker AXS D8 Discover X-ray diffractometer (XRD). The film growth process was monitored by reflection high energy electron diffraction (RHEED).

2.2.1 Transmission electronic microscopy

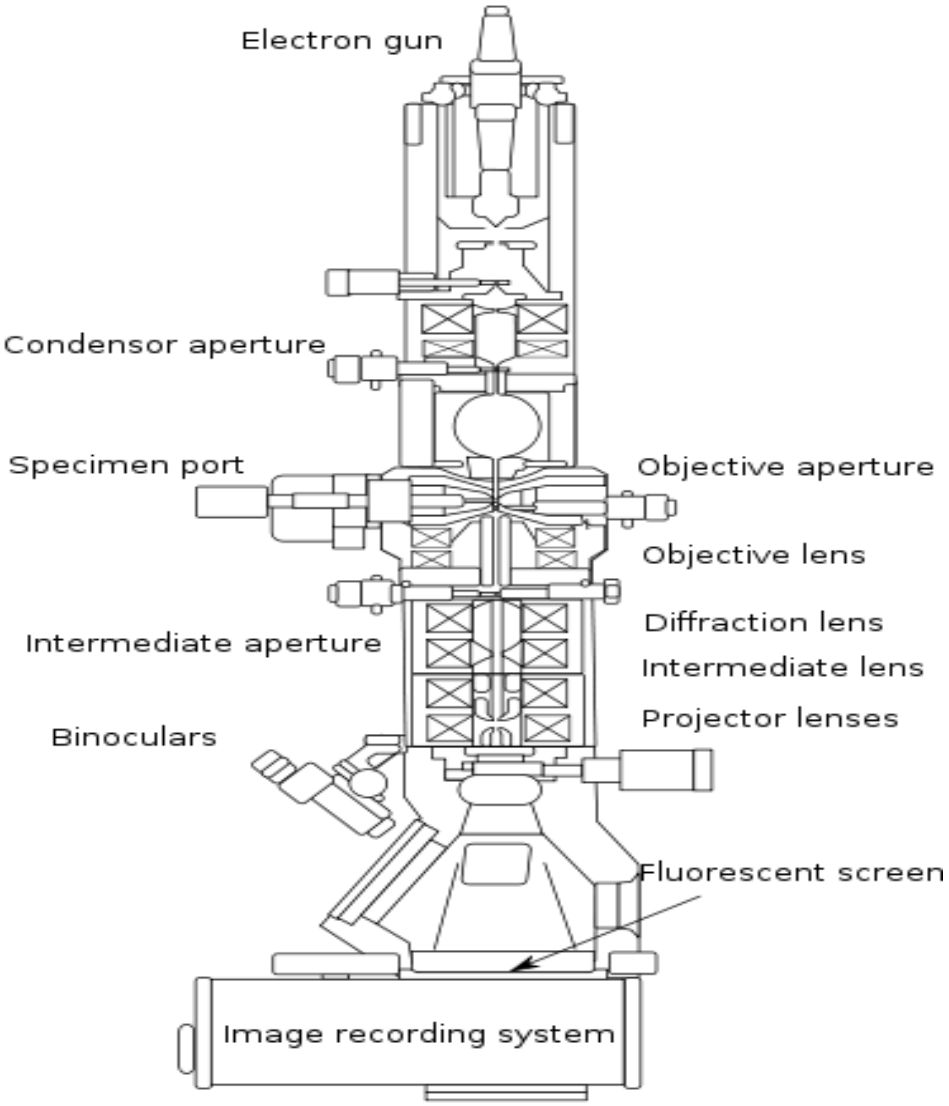

Fig.2.3 Schematic diagram of a TEM

Transmission electron microscopy (TEM) is a powerful technique for structural characterization. As shown in Fig.2.3, a beam of electrons is focused by a series of electromagnetic lenses, and transmitted through ultra thin specimen (approximately 50 nm), and an image of the interested area can be formed from the transmitted and diffracted electron beam by the objective lens. The image is then magnified

and focused onto an imaging plate for instance a fluorescent screen and a charge-coupled device (CCD) camera. The main imaging, diffraction and spectroscopy techniques in TEM include: 1. Conventional imaging (bright-field and dark-field TEM); 2. Electron diffraction (selected area electron diffraction, SAD); 3. Phase-contrast imaging (high-resolution TEM, HRTEM); 4. Electron energy loss spectroscopy; 5. Energy dispersion X-ray (EDX). A JEM-2010 TEM was used for film structure characterization which was operated at 200 kV, with high-resolution, SAD and EDX functions. Cross-section TEM samples of the $LuFe_2O_4$ films were made by mounting the films face by face, followed by mechanical polishing and dimpling down to a thickness of about 10 μm and then ion milling.

2.2.2 X-ray diffraction

X-ray diffraction (XRD) is a sophisticated, non-destructive technique to characterize the crystalline phase and structural properties in solid materials. The intensity received from interaction between X-ray and periodic geometry of crystals at a certain angle is record and analyzed. Figure 2.4 shows the basic working principle of XRD. When a beam of parallel X-rays incident on the crystal surface at an angle θ, diffraction occurs at the same angle θ as the regular structure with its repeating distance satisfies the Braggs's Law:

$$2d_{hkl}\sin\theta=\lambda \quad \text{.....(2.1)}$$

where the d_{hkl} is the distance of the lattice plane (hkl) and θ is the angle as shown in Fig.2.4 and λ is the wavelength of X-ray.

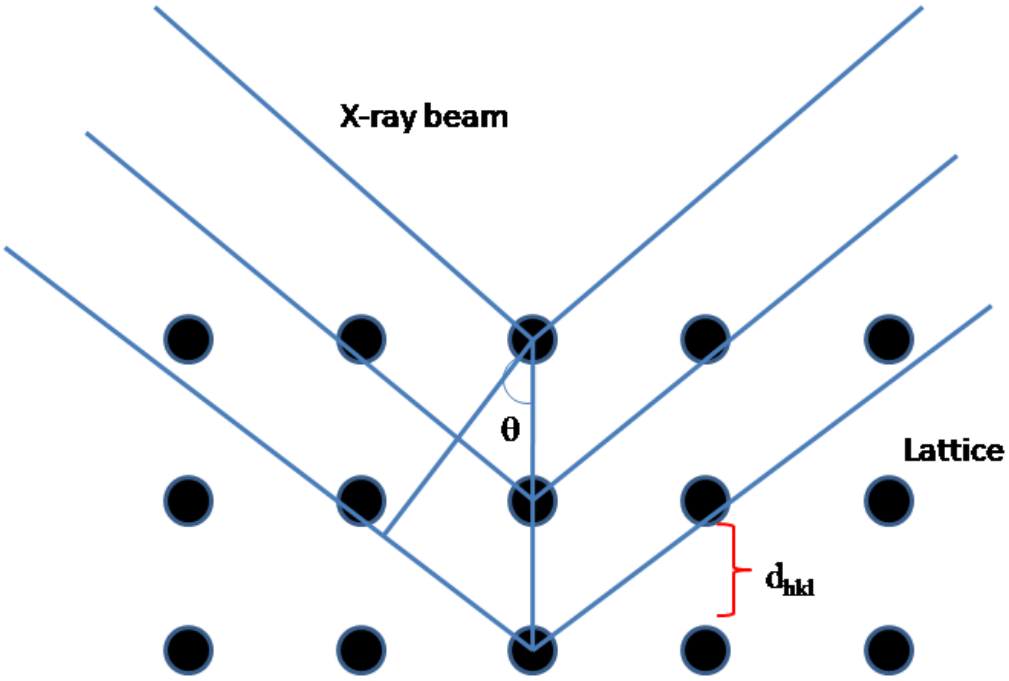

Fig.2.4 Schematic diagram of the XRD.

In our experiment, XRD analysis of the $LuFe_2O_4$ films was carried out on a Bruker AXS D8 discover X-ray diffractometer. A horizontal high-resolution ω-2θ goniometer is installed in this four circle X-ray diffractometer. Two additional axes of rotations are provided by an open Eulerian cradle (-90° < ψ < 90°, and -360° < φ < +360°). A Cu made long-fine-focus, ceramic X-ray anode tube is used as the X-ray source. In normal operation, the power we used is 40 kV and 40 mA, and Cu Kα radiation with a wavelength λ = 0.154 nm is used with a Cu filter. X-ray structural analysis is used to identify the epitaxial structure of the thin films. The analysis techniques include ω-2θ scans, *Φ* scans, and rocking curves. ω-2θ scans can be performed to determine the orientation of crystalline phase in the thin films. *Φ* scans are used to characterize the epitaxial feature of the films. Rocking curve determines

the full width at half maximum (FWHM) of the chosen peak and provide the information of the orientation distribution of the grown film.

2.3 Electrical Properties Characterization

Electrical properties of $LuFe_2O_4$ films were measured by HP Aglient Impedance Analyzer 4294A for frequency range from 40 to 110 MHz, and 4291B RF for high frequencies from 1 MHz to 1.8 GHz. Temperature-dependent dielectric measurement was also performed. Inter-digital (IDT) electrodes were used for electrical property measurement of the film. The IDT electrodes were made by sputter deposition of Au on the film followed by photolithography and chemical etching.

The 4291B RF impedance analyzer was calibrated before each measurement. Calibration standard of “open”, “short”, “50Ω load” and “low-loss capacitor” were used in the calibration process. Following this, impedance standard substrates, including “open”, “short” and “50W load”, provided by probe station manufacturer were used to remove parasitic effect from the probe and connection wire. After calibration, the sample was placed on a standard probe station Microtech RF-1. The probe used in the measurement was SG gold probe. The whole set up of experiment apparatus is shown in Fig.2.5.

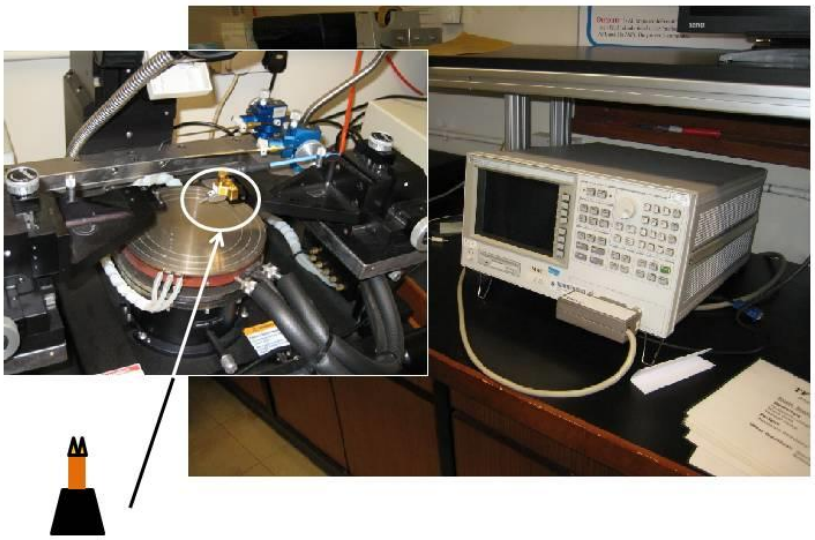

Fig.2.5 A picture of HP 4291B RF impendent analyzer with an inset picture of probe station and SG gold probe.

2.3.1 Au IDT electrode synthesis

Gold electrode film was deposited by dc magnetron sputtering which is a widely used technique for thin film deposition. The detailed condition of the deposition is listed in Table 2.1

Table 2.1 Deposition condition of Au film

Target	Au
DC power	70 W
Substrate Temperature	300 ℃
Sputtering gas	Ar 10(sccm)
Gas pressure	35 mTorr
Thickness	100 nm
Deposition time	9 min

The Au film is then patterned by photo-lithography to become an inter-digit electrode. There are various steps involved in photolithographic processing. In this work, Aligner 800MBA is used for photo mask exposure. Fig.2.6 shows the details of photolithography and etching process in clean room.

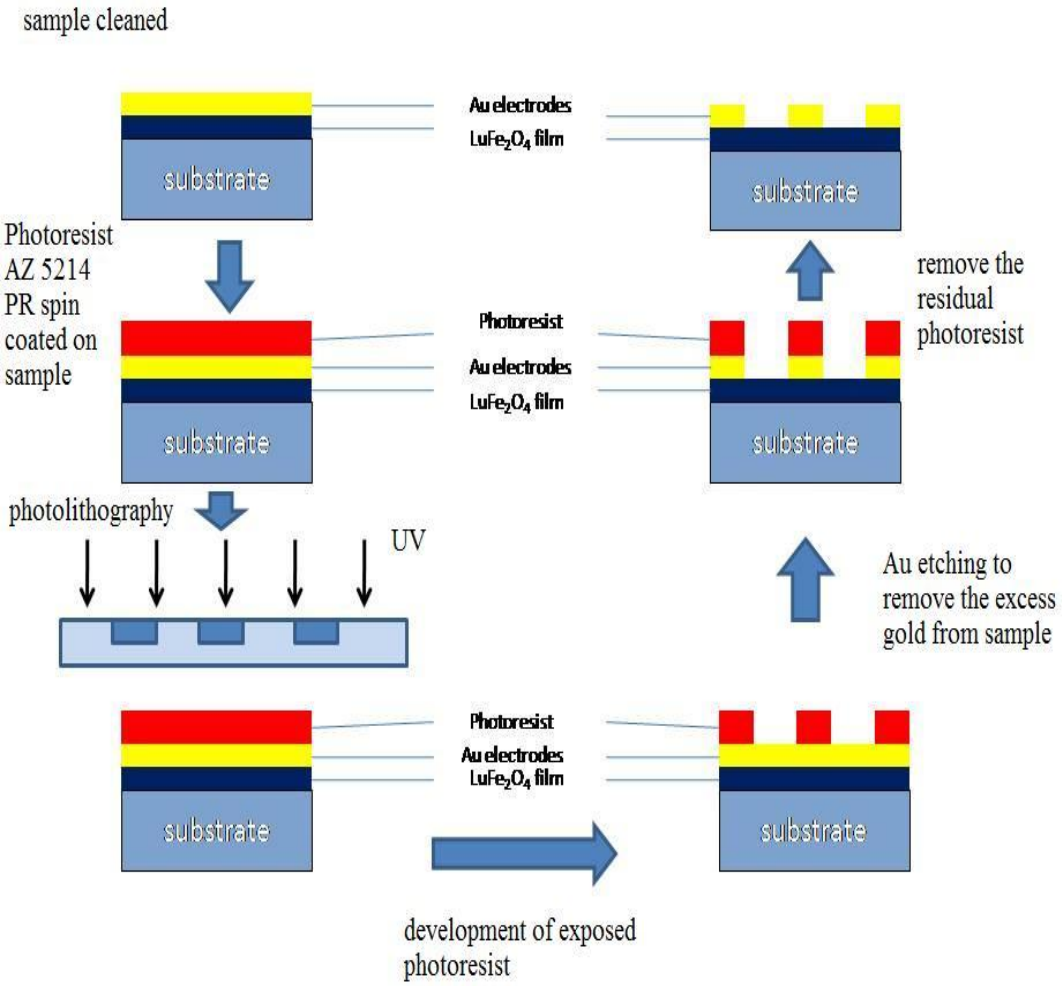

Fig.2.6 Schematic diagram of the working process to make an IDT electrodes

Before Au film deposition, the sample was cleaned by ultrasonic bath of acetone and ethanol for washing out organic, ionic and metallic particles and other impurities. Dried by compressed air, the sample with Au film was spin coated with a positive photoresist (AZ 5214 PR Clariant) for 60 min at 4000 rpm, forming a 1 μm uniform film. The photoresist film was then put on a heater baking at 100 ^{o}C for 1 min. Through the use of aligner, all portion of the film was exposed under UV light for 15

seconds except those parts protected by inter-digital capacitor pattern. Samples were then immersed in a developer solution (AZ 300 MIF developer) for 1 min to remove the unprotected photoresist layer. The patterns were checked under optical microscopy before going to next step. After rinsed by the de-ionized water and dried by a stream of compressed air, the gold film was then removed by using Au etching solution (KI and I_2 solution diluted by water) for 30 seconds with electrodes protected by photoresist remained. The electrode pattern should also be inspected by optical microscopy before removing the photoresist protective layer by acetone.

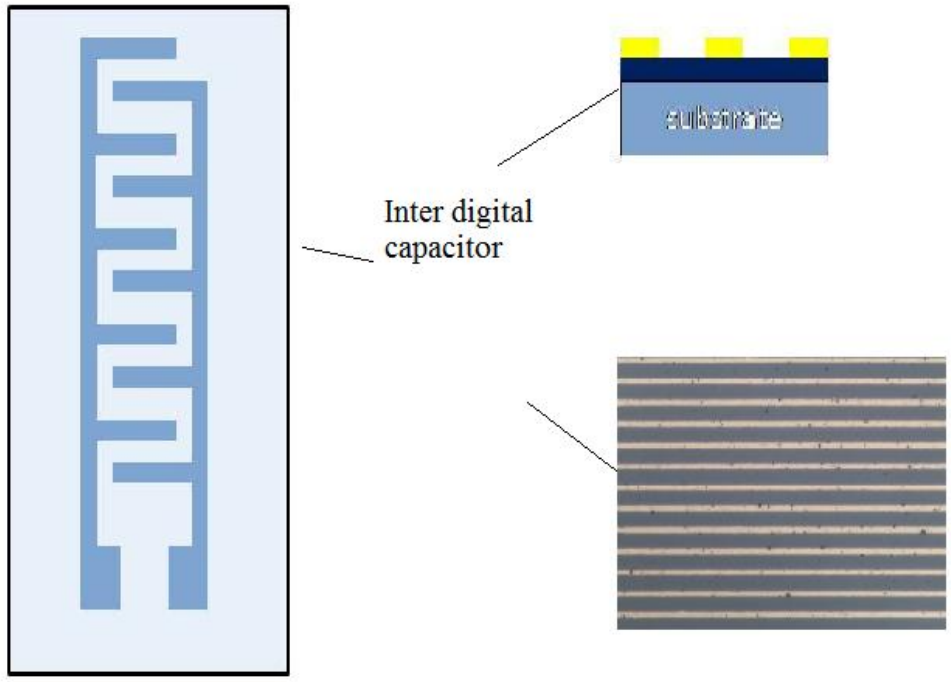

Fig.2.7 Diagram of IDT electrode geometry

Fig.2.7 shows schematic diagram of the inter-digital capacitor (IDC) electrodes

geometry. In my experiment, the IDC electrodes were used for ferroelectric and dielectric characterizations. There are two kinds of IDC patterns we used in the measurements. One has 40 fingers with finger length 1.5 mm and finger width 1 μm for HP 4294A and HP 4194A, the other has 90 fingers with finger length 1 mm and finger width and 1.5 μm, respectively, for HP 4291B. (YOU USE 10 um width??)

2.4 Magnetic Property Characterization

Vibrating sample magnetometer (VSM) is a widely used scientific instrument to measure magnetic properties of magneto-materials such as diamagnetic, paramagnetic, ferromagnetic and antiferromagnetic. The typical setup of VSM is shown in Fig.2.8. There is a sample holder with the sample fixed at the end of the sample rod. The other head of the rod is connected to an electromechanical transducer with an oscillation frequency of 90 Hz. The sample and sample holder are placed deep into a chamber which is filled with liquid nitrogen and with a temperature control system, including heater and PID feedback system. Besides the chamber, there are two electromagnets that induce magnetic dipoles in the sample which can be measured by a pick-up coil. The signal output from the coil will be analyzed and recorded by the computer. In my project, Lakeshore 736 VSM was used for magnetic property characterization of the $LuFe_2O_4$ films. Before measurement the driver should be warmed up for at least 24 hour to ensure that there is no height drifting. The system was also calibrated by

standard sample before measurements.

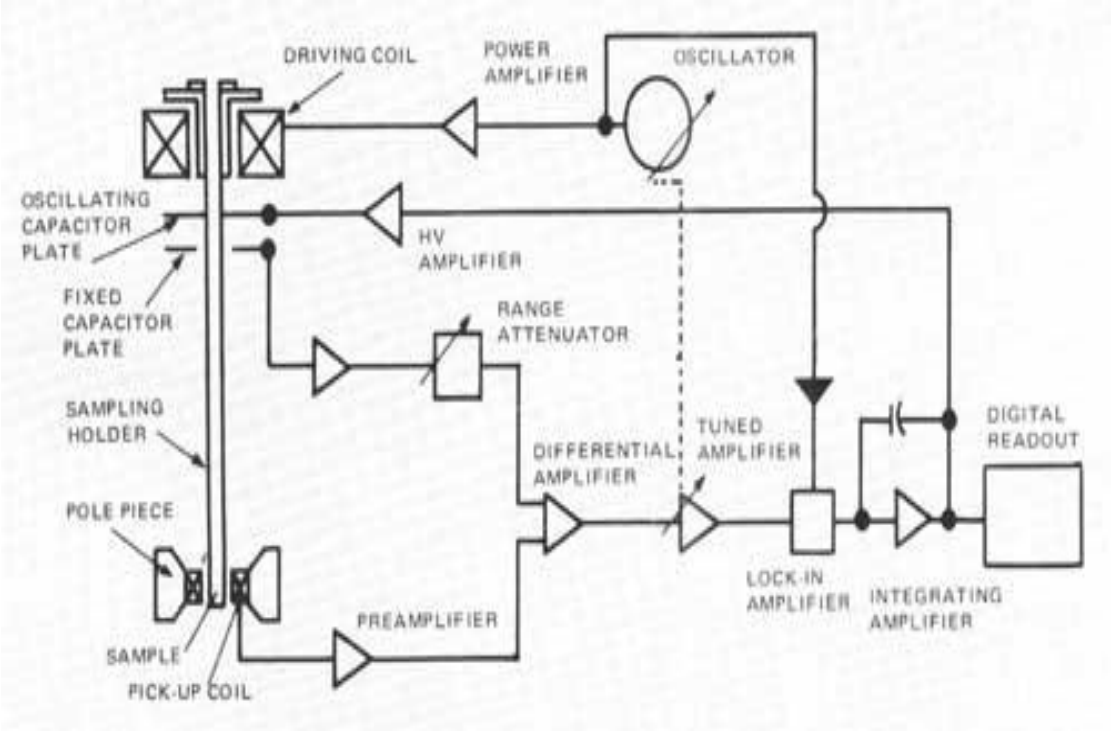

Fig.2.8 Schematic diagram of VSM working process

Chapter 3 Growth and Structural Characterization of $LuFe_2O_4$ Thin Films

3.1 Introduction

To grow $LuFe_2O_4$ film is one of the key tasks in this thesis. The nature of the $LuFe_2O_4$ structure, i.e., the equivalent positions and ratio of Fe^{2+} and Fe^{3+}, makes it very difficult to form $LuFe_2O_4$ phase in the film. In addition, the existence of variant structures of $LuFe_xO_y$ makes it more complicated in structural characterization. In this chapter, the detailed growth conditions and the film structural characteristics are introduced.

PLD method was chosen for $LuFe_2O_4$ thin film growth due to its advantages in growing high-quality oxide films and a wide range of parameters for controlling film properties. Substrate temperature, laser frequency and target composition are the three main parameters need to be optimized for $LuFe_2O_4$ film growth, in which the substrate temperature is found to be essential for the formation of $LuFe_2O_4$ phase in the film. $\omega/2\theta$ XRD scan was used to characterize the crystallization and orientation of the $LuFe_2O_4$ film. XRD Φ scan was employed to determine the epitaxial growth of the $LuFe_2O_4$ film. Crystal structures of the $LuFe_2O_4$ film as well as the interfacial structure between film and substrate were studied by means of HRTEM and SAED.

3.2 Growth of $LuFe_2O_4$ films on (0001) sapphire substrates

In this project, (0001) sapphire (Al_2O_3 single crystal) substrate was used for $LuFe_2O_4$ film deposition. Sapphire has a hexagonal structure with a = 4.758 Å and c = 12.991 Å. The lattice mismatch in a-b plane between $LuFe_2O_4$ and sapphire is 32%; while a =3.438 Å and c =25.28 Å for $LuFe_2O_4$. The small dielectric constant, low loss tangent and high resistance of sapphire make it a promising candidate for ferroelectric thin film growth and characterizations.

Prior to deposition, the substrate was pre-cleaned by acetone and ethanol to remove organic contaminations on the surface, and then dried by compressed air. The laser used in the deposition is KrF (λ=248 nm) excimer laser with an energy density of 3-4 J/cm^2. Ceramic discs of Lu_2O_3 and Fe_2O_3 powders with composition ratios of 1:2, 1:3 and 1:4 were used as target for PLD growth. During the deposition process, the target was rotated to reduce non-uniform erosion. The substrate was placed parallel to the target at a distance of 7 cm. During deposition, the chamber was kept at high vacuum of 1x10^{-5} Pa. The deposited films were then *in-situ* annealed at high temperature (750-850 ℃) in an ambient of oxygen pressure (up to 10 Pa) for 30 min to 1 hour; while high-purity oxygen gas was used as reactive agent introduced into the chamber through a needle valve. This annealing process may ensure oxygen stoichiometry ratio of Fe^{2+} and Fe^{3+} in the films. Finally, the film was cooled down to room temperature slowly.

Fig.3.1 Setup of Laser-MBE system used in our experiment.

The reason to use different target composition rather than stoichiometry one is that there is evidence of interfacial reaction consuming Fe and results in Fe deficient $LeFeO_x$ phase in the films. The advantages and disadvantages of Fe-enriched target will be discussed by comparing of the crystallization in the $LuFe_2O_4$ films. Condition of film deposition on (0001) Al_2O_3 substrate with best crystallization is listed in Table 3.1.

Table 3.1 Deposition condition for $LuFe_2O_4$ thin film

Target	Lu:Fe=1:4
Laser density	3 J/cm^2
Laser frequency	1 Hz
Substrate temperature	850 ^{o}C
Vacuum pressure	1x10^{-4} Pa
Deposition time	1 hr

3.3 Structural characterization of the $LuFe_2O_4$ films

3.3.1 Microstructure of the $LuFe_2O_4$ films

To characterize the crystal orientation of the $LuFe_2O_4$ film on (0001) sapphire substrate, X-ray diffraction study of the film was carried out. Figure 3.2 shows the XRD result of the $LuFe_2O_4$ film grown under optimized condition as shown in Table 3.1, in which the three highest peaks can be identified as (0003), (0006) and (0009) atomic planes of $LuFe_2O_4$. Planes of (0,0,0,15), (0,0,0,18), (0,0,0,21) may also be identified from the XRD pattern, but the intensity of peaks are very weak. From this XRD result, $LuFe_2O_4$ film shows c-axis epitaxial growth on the (0001) sapphire substrate. The full width at half maximum (FWHM) of the $LuFe_2O_4$ (0009) peak scanned by a rocking curve is 0.45^o, as shown in the insert of Fig.3.2. There are also several weak peaks which can be attributed to Fe_3O_4 (111), (222), (333), while the peak at 64^o may also belongs to $FeAl_2O_4$ (440), indicating an interfacial reaction, which will be discussed in chapter 3.4. This indicates impurity phases of Fe oxides forming in the film as a drawback of using Fe-enriched target.

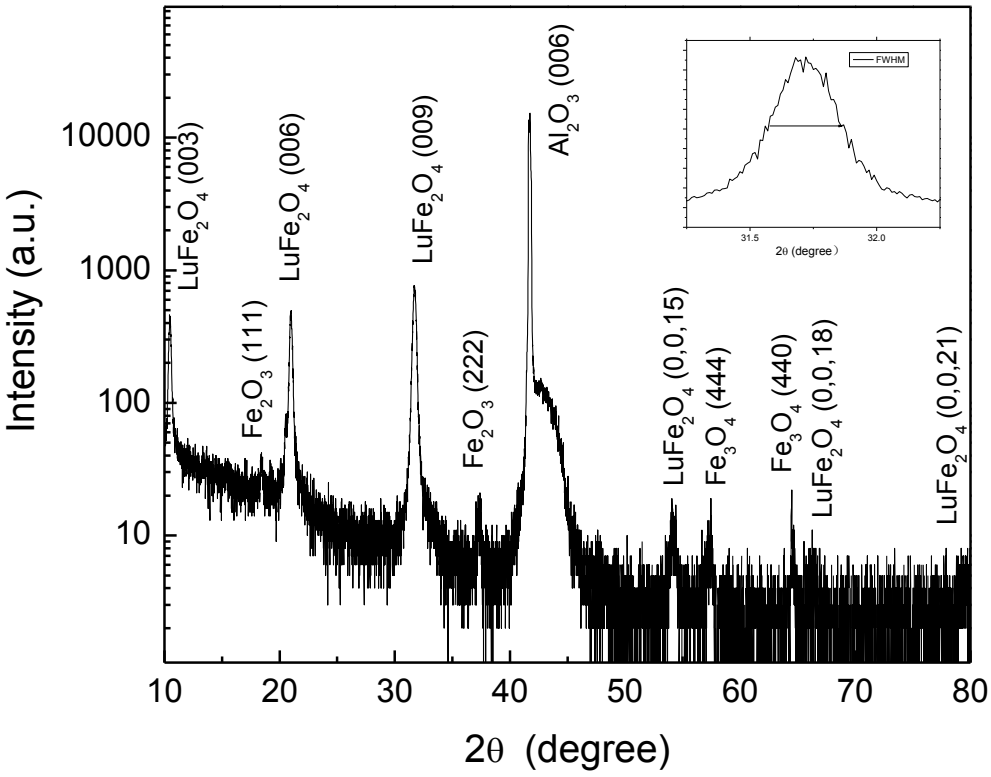

Fig.3.2 XRD ω-2θ pattern of $LuFe_2O_4$ thin film on (0001) sapphire substrate under optimized condition. The insert is rocking curve of $LuFe_2O_4$ (0009) diffraction peak.

To further confirm the epitaxial growth, Φ-scan was performed to determine the lattice matching between the film and substrate. Fig.3.3 is the XRD Φ-scan result in which the lattice plane $(20\bar{2}2)$ of Al_2O_3, $\chi = 72.43^o$, and lattice plane $(10\bar{1}1)$ of $LuFe_2O_4$, $\chi = 83.27^o$, were used. From the Φ-scan result, the peaks of $LuFe_2O_4$ and Al_2O_3 are totally matched in the same position, proving that the lattice structure of $LuFe_2O_4$ film is grown on Al_2O_3 epitaxially. The 60^o interval between peaks of $LuFe_2O_4$ film suggests a six-fold symmetric structure in comparison with the three-fold symmetric structure of Al_2O_3 substrate with interval of 120^o.

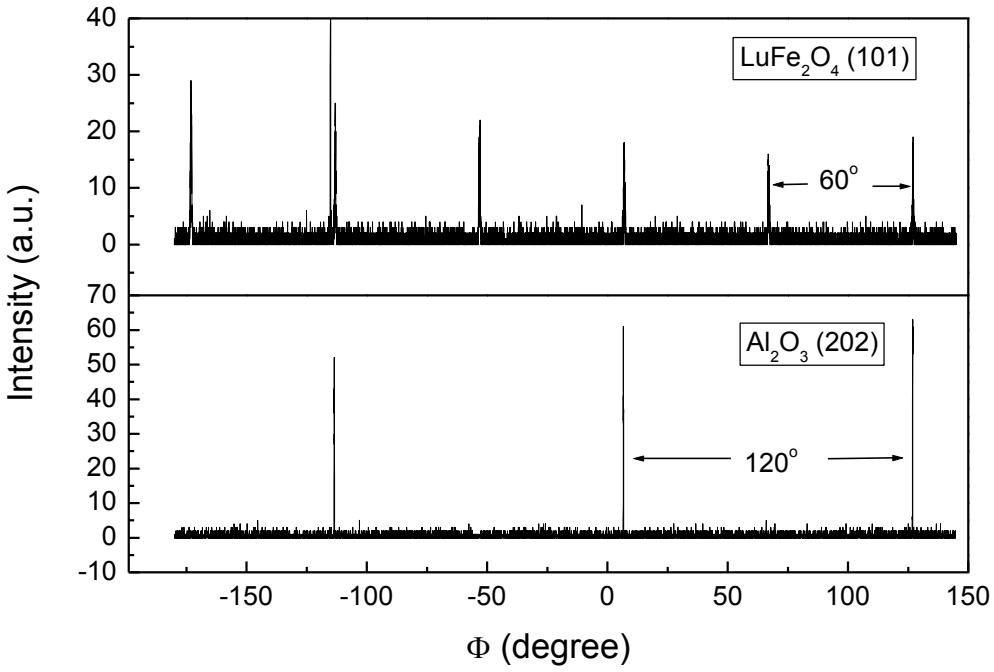

Fig.3.3 Φ-scan of $LuFe_2O_4$ thin film on (0001) sapphire at $(10\bar{1}1)$ plane.

3.3.2 Interfacial structure characterization by TEM

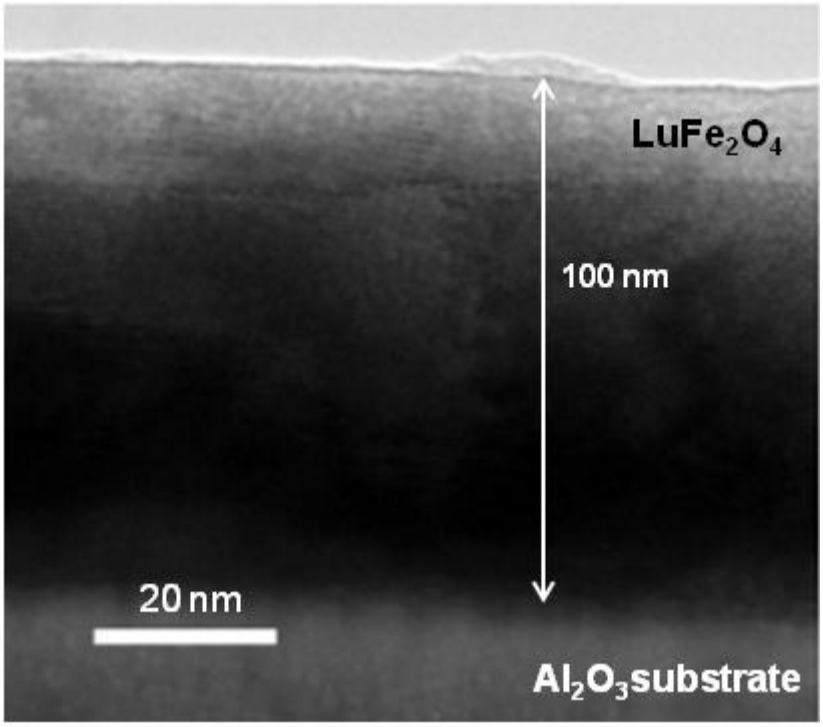

Fig.3.4 Low magnification TEM image of the $LuFe_2O_4$ thin film.

Cross-sectional TEM study was carried out to characterize the microstructure of the $LuFe_2O_4$ film and also the interface between film and substrate. Low magnification TEM image is shown in Fig.3.4. One can see that, the thickness of $LuFe_2O_4$ thin film is 100 nm, where a deposition rate of 0.26 Å/pulse can be determined. The film is flat at the surface but the interface is not sharp, suggesting that interfacial reaction phase may exist.

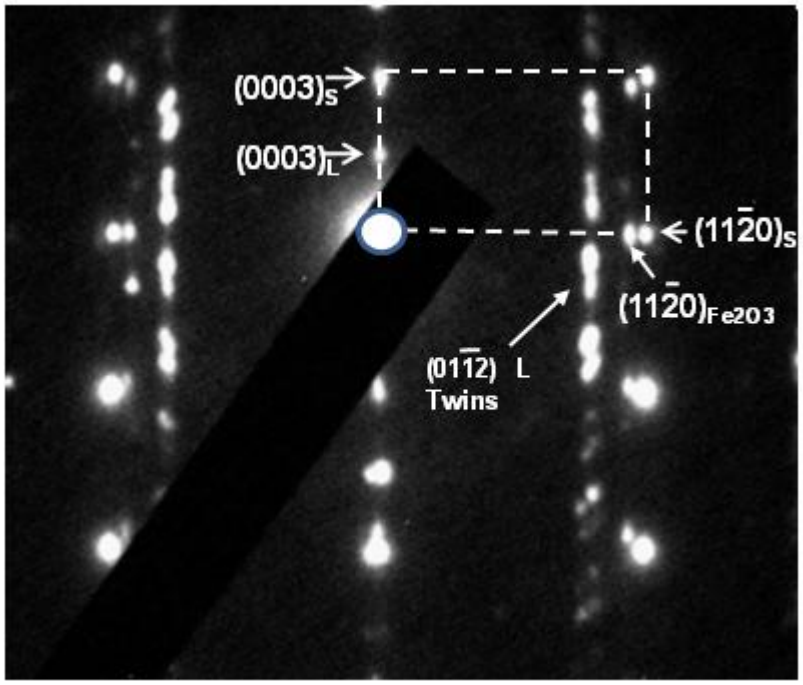

Fig.3.5 Composite diffraction pattern of the film and Al_2O_3,substrate, where S stands for substrate and L stands for $LuFe_2O_4$.

The Fig.3.5 is the composite diffraction pattern including all the film area and the substrate. In this diffraction pattern, it is found that the $LuFe_2O_4$ (0003) spot is in the half way of Al_2O_3 (0003) spot, which is perfectly consistent with the fact that the lattice parameters of $LuFe_2O_4$ c=25.28 Å is roughly double of that of Al_2O_3 which is c=12.99Å. The twin spots are believed to be (01$\bar{1}$2) of $LuFe_2O_4$. The spots beside to Al_2O_3 spots are confirmed to be Fe_2O_3 impurity phase due to the Fe-enriched target. Fe_2O_3 possesses a similar structure with Al_2O_3, but with a relatively larger value of lattice parameters a and c, compared to Al_2O_3.

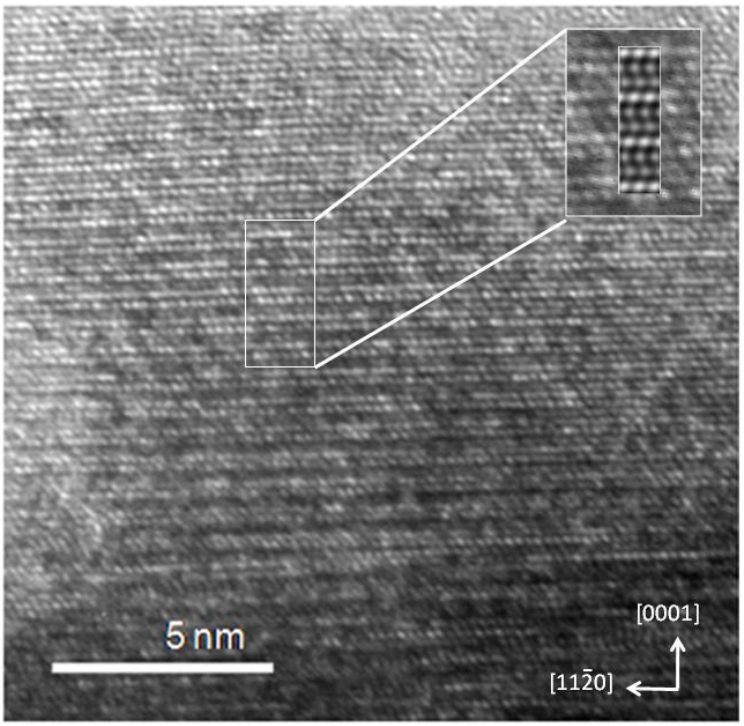

Fig. 3.6 HRTEM image of $LuFe_2O_4$ unit structure.

Figure 3.6 is a HRTEM image of the $LuFe_2O_4$ film on sapphire substrate observed along the [01$\bar{1}$0] direction of Al_2O_3. Apparently the phase in $LuFe_2O_4$ thin film presents a typical crystal lattice, where between every two layers of Lu-O, there are two layers of Fe-O. The lattice image in the inset picture of Fig.3.6 from the $LuFe_2O_4$ film matches well with the simulated image from Ref. [Y. Zhang, 2007], where the distance of the *c* atomic plane of $LuFe_2O_4$ can be identified as 25.46 Å.

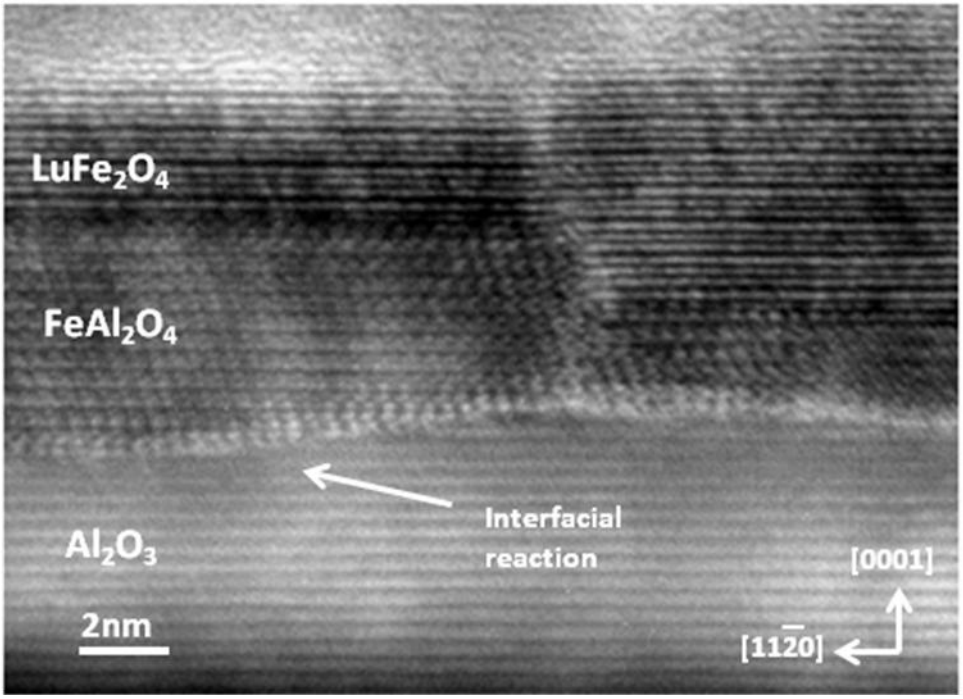

Fig.3.7 Typical interfacial structure of $LuFe_2O_4$ thin film was deposited on Al_2O_3 by Fe-enriched target. Dislocation is also found in the film and imperfect surface of Al_2O_3 implies interfacial reaction at high temperature.

However, there is an interfacial layer as shown in Fig.3.7 between the $LuFe_2O_4$ film and sapphire substrate. As suggested by the XRD results, this interfacial reaction layer should either be $FeAl_2O_4$ or Fe_3O_4. Since $FeAl_2O_4$ and Fe_3O_4 possess very similar crystal structure and lattice constant, these two structures cannot be distinguish by analyzing HRTEM image and selected area diffraction patter. Nevertheless, the rough surface of Al_2O_3 suggests that, this interfacial phase is a reaction result between Fe oxide and Al_2O_3 which is $FeAl_2O_4$ as reported [T. O. Mason, 2006]. The grain boundary and stacking fault can also be observed in Fig.3.7. The formation of staking fault dislocation in $LuFe_2O_4$ is due to the strain induced by the rough surface of Al_2O_3 substrate, which is caused by interfacial reaction.

In order to determine the interfacial phase, electron microscopy simulation of the $FeAl_2O_4$ and Fe_3O_4 structures was performed. Figure 3.8 shows the atomic projection

diagrams of $FeAl_2O_4$ and Fe_3O_4 structures, where both of them possess rhombouhredral structure and the lattice constants are 8.155 Å and 8.394 Å for $FeAl_2O_4$ and Fe_3O_4, respectively. The simulated HREM images and diffraction patterns of $FeAl_2O_4$ and Fe_3O_4 are shown in Figs.3.9 and 3.10. A clearer HRTEM image close to the interface area is shown in Fig. 3.11. By comparing these figures, one can see that the interfacial layer in HRTEM image is more likely $FeAl_2O_4$ other than Fe_3O_4.

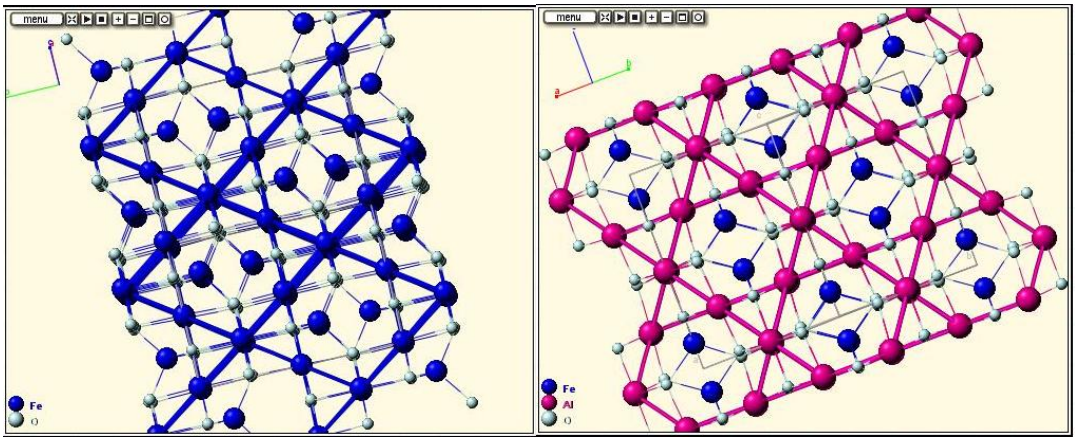

Fig.3.8 Diagram of atomic projection of Fe_3O_4 (left) and $FeAl_2O_4$ (right) structures. The observation direction is along [110] of the rhombouhredral structure.

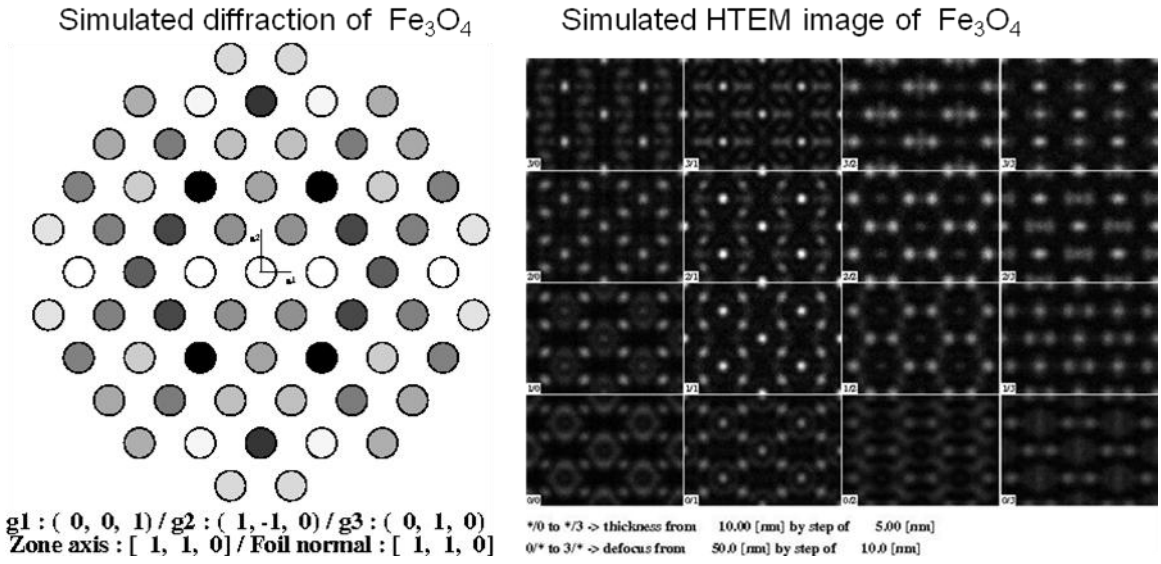

Fig.3.9 Simulated diffraction pattern and HREM image of Fe_3O_4 structure. The

observation direction is along [110] of the spinal structure.

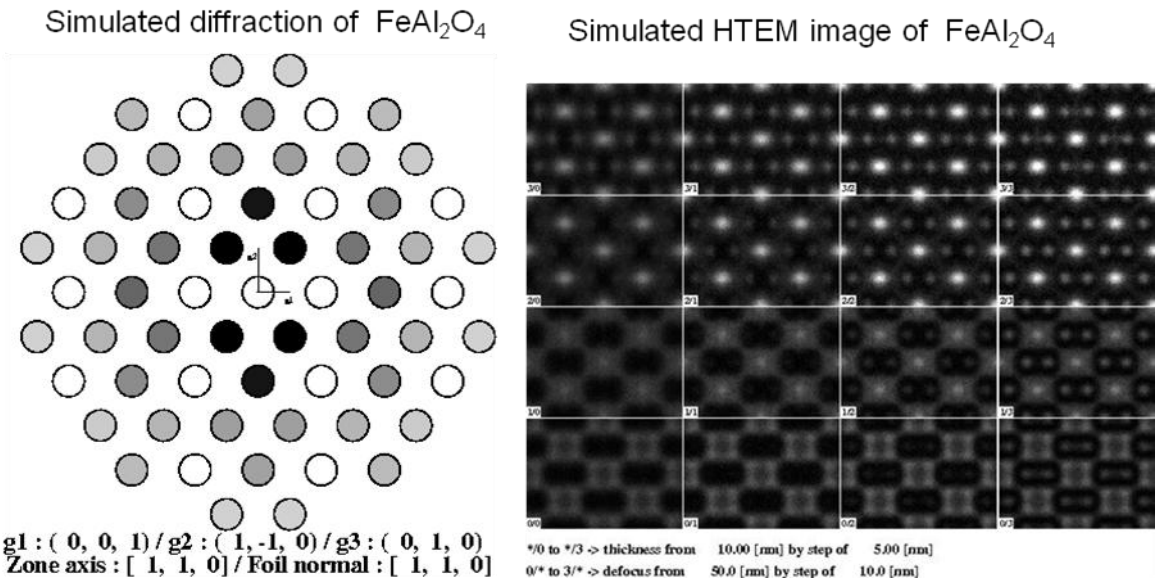

Fig.3.10 Simulated diffraction pattern and HREM image of $FeAl_2O_4$ structure. The observation direction is along [110] of the rhombouhredral structure.

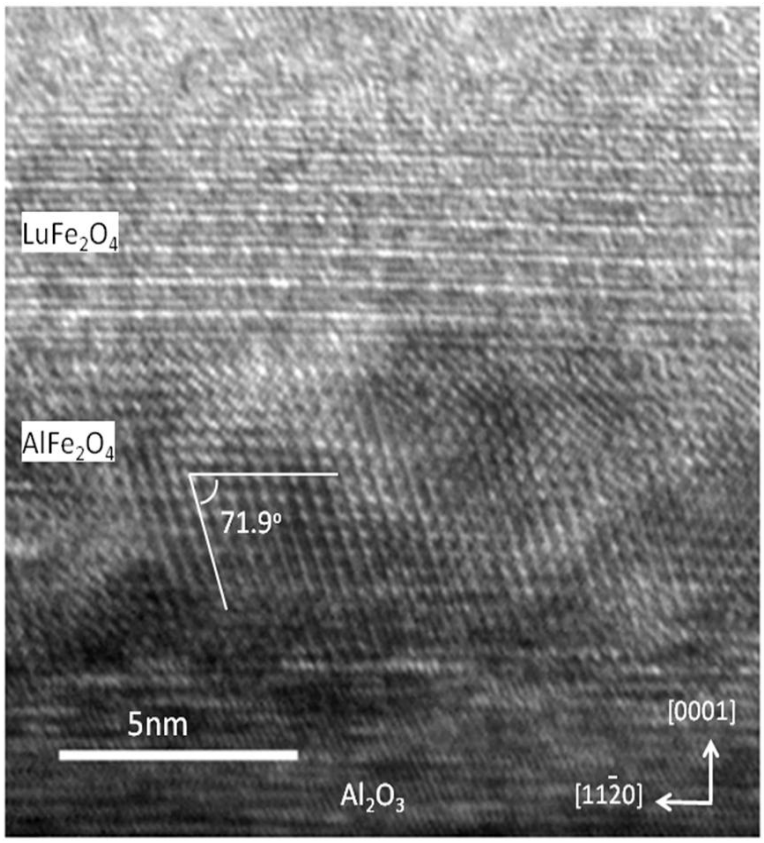

Fig. 3.11 Cross-sectional HRTEM image of the $LuFe_2O_4$ film on (0001) sapphire close to the interface area. The observation direction is along the $[01\bar{1}0]$ of sapphire and

$LuFe_2O_4$.

Selected area diffraction is used to further prove our interpretation about the HRTEM results and simulations. Fig.3.12 is a SAED pattern corresponding to an area, where there are only substrate and a thin interfacial layer. This composite diffraction pattern can be indexed as along the $[01\bar{1}0]Al_2O_3//[110]FeAl_2O_4$. The in-plane orientation relationship between the $FeAl_2O_4$ and Al_2O_3 can be determined as $(0001)Al_2O_3//(111)FeAl_2O_4$.

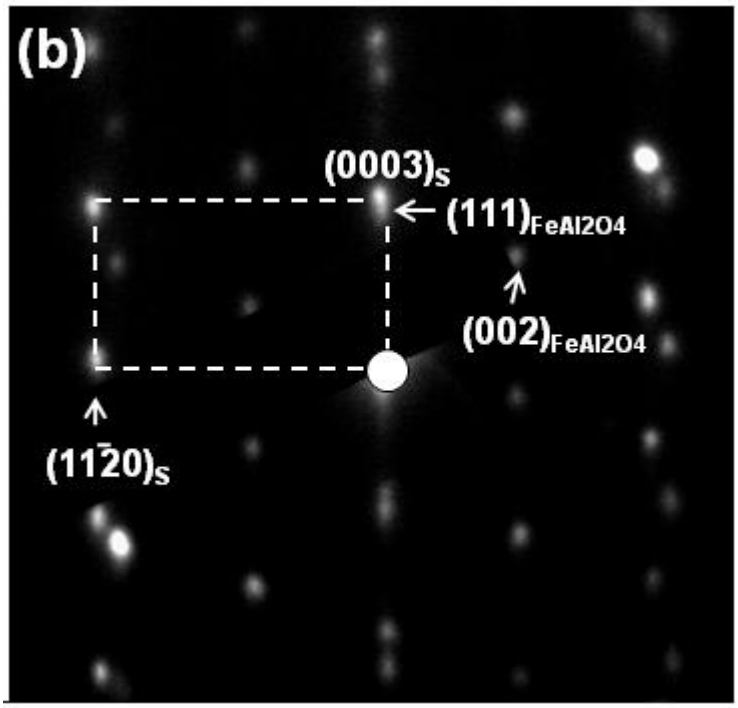

Fig.3.12 Composite SAED pattern of the Al_2O_3 substrate and $FeAl_2O_4$ interfacial reaction phase. The zone axis is along the $[01\bar{1}0]_{Al2O3}//[110]_{FeAl2O4}$ direction.

It can be concluded that the interfacial reaction happens at the earlier stage of the film growth at high temperature, while Fe diffuses into the Al_2O_3 substrate and form the reaction phase. Fe-enriched target provides a right ratio of Lu:Fe after some Fe is consumed. However, the low magnification TEM image of Fig. 3.4 shows that the

upper layer of the film has a relatively brighter contrast which may be due to the content of more Fe than the normal ratio in $LuFe_2O_4$. Fe_2O_3 was also found from the electron diffraction pattern. The Fe_2O_3 interfacial layer was only observed in Fe-enriched target; while $FeAl_2O_4$ was also found in the film deposited by stoichiometry target.

3.4 Optimization of the $LuFe_2O_4$ films growth condition

In order to grow high-quality $LuFe_2O_4$ film, parameters such as substrate temperature, oxygen partial pressure, laser frequency and target composition need be optimized. In our experiment, as previously mentioned, the vacuum condition was of 10^{-5} Pa in deposition process, and the oxygen pressure was 10 Pa during in-situ annealing process. Excimer laser (Lamda Physik 205) with a wavelength of 248 nm was utilized to irradiate on the target in forming a high-energy plume of atomic particles. The laser energy used was 3-4 J/cm^2, and the laser frequency was fixed at 1 Hz. A series of experiments were carried out to investigate the growth condition of $LuFe_2O_4$ film, and the influences of the growth parameters, including target composition and substrate temperature. The detailed results are discussed as below.

A. Relation between target composition and film structure

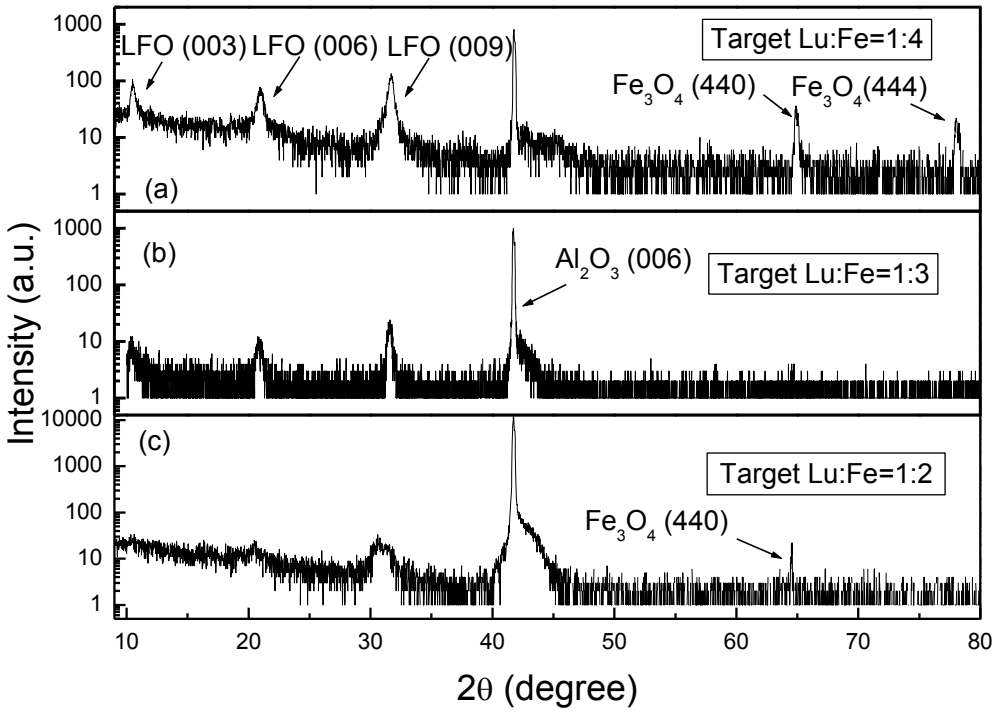

Fig.3.13 XRD patterns of $LuFe_2O_4$ thin films deposited using targets with different Lu:Fe ratios.

Figure 3.13 shows XRD patterns of the $LuFe_2O_4$ films deposited using targets with different Lu:Fe ratios. The deposition was under vacuum condition of 10^{-5} Pa and the growth temperature for these samples was 750°C with pulsed frequency at 1 Hz. One can see from Figs.3.13 (a) and (b) that with a Fe-enriched target the XRD pattern shows strong characteristic peaks of (0003), (0006) and (0009) of $LuFe_2O_4$; while under the same deposition condition, by using stoichiometry $LuFe_2O_4$ target with Lu:Fe=1:2, the peaks of $LuFe_2O_4$ (000*l*) are very week in the XRD pattern as shown in Fig.3.13 (c). However, one can see that with a Fe-enriched target, impurity phase of Fe_3O_4 appears in the film as shown in Fig.3.13 (a). It is worth noting that the peaks of the Fe_3O_4 in Figs.3.13 (a) and (c) may also belong to $FeAl_2O_4$, which has a very similar crystal structure with Fe_3O_4 and is believed to be formed by interfacial reaction between Fe-O and Al_2O_3 substrate. Since the interfacial reaction consumes Fe

element, the extra amount of Fe in the target can compensate the loss of Fe and therefore favors the formation of $LuFe_2O_4$ phase in the film. In fact, before using the Fe-enriched target, all trials to grow the $LuFe_2O_4$ film failed and only some $LuFeO_x$ phases can be formed. This motivated us to use Fe-enriched target, and eventually $LuFe_2O_4$ film deposition was realized. This interfacial reaction enhanced $LuFe_2O_4$ film growth mechanism has been illustrated by the transmission electron microscopy (TEM) study in previous section.

Figure 3.14 shows the XRD pattern of the film with the stoichiometry $LuFe_2O_4$ ceramic target, where it can be seen that besides the $LuFe_2O_4$ phase, Lu_2O_3 phase appears in the XRD patterns. This can be an evidence for the hypothesis of the deficiency of Fe and the excess of Lu in deposition process, which results in the formation of Lu_2O_3 phase.

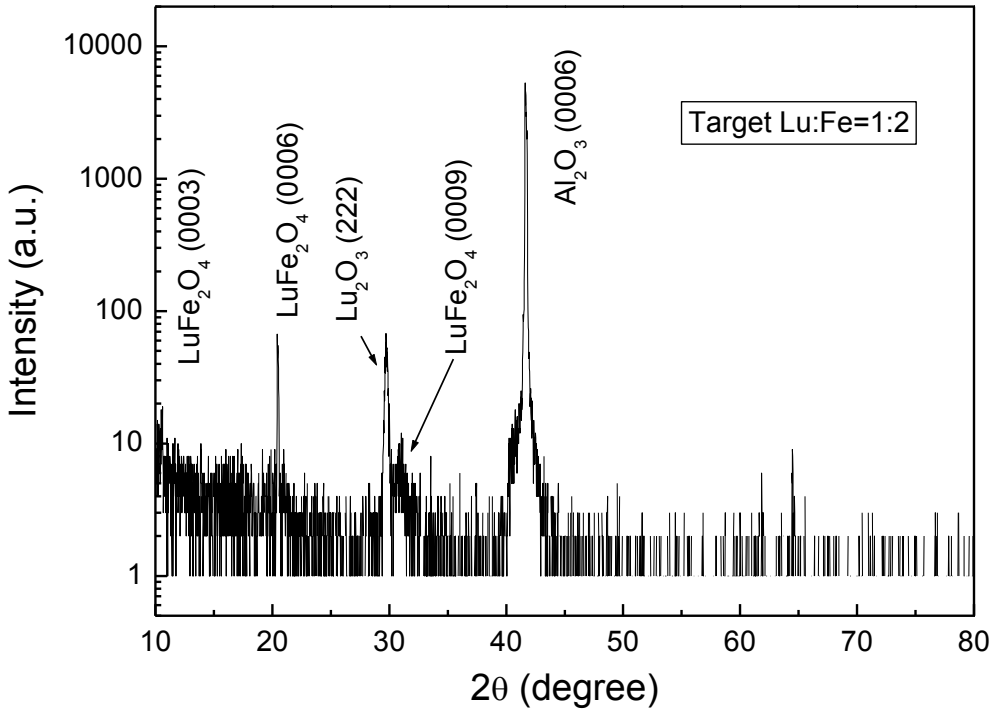

Fig.3.14 XRD 2θ scan result from the $LuFe_2O_4$ film deposited with stoichiometry $LuFe_2O_4$ target. Two groups of peaks can be seen.

B. Substrate temperature effect

Among all the growth conditions, the substrate temperature is found to be the most critical condition. Figure 3.15 shows the XRD patterns of the $LuFe_2O_4$ films deposited at different temperatures using a target with Lu:Fe ratio of 1:4, and pulse frequency at 1 Hz. It is apparent that at substrate temperature lower than 650^{o}C, the grown film is basically amorphous, as shown in Fig.3.15 (c); while at 750^{o}C (Fig.3.15 (b)) the film is crystallized but XRD pattern shows relatively weaker peaks. Therefore, we can conclude that, 750 ^{o}C is a critical temperature for the growth of the $LuFe_2O_4$ film, below which the film quality is relatively poorer. As shown in Fig.3.15 (a), the film grown at 850^{o}C presents better crystallization with stronger peaks in XRD patterns, however, at this temperature, another impurity phase Fe_2O_3 can be identified.

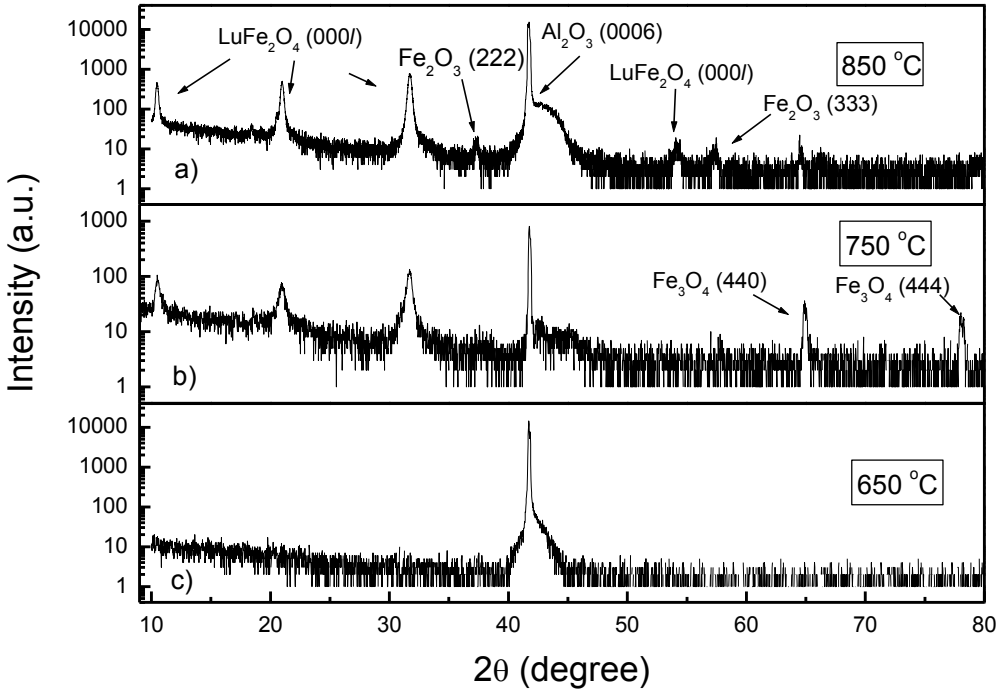

Fig. 3.15 XRD patterns of the deposited films at different temperatures.

C. Pulsed-laser frequency

The laser frequency is also an essential parameter to the $LuFe_2O_4$ film growth. The low frequency of laser pulse provides a long relaxation time for adatom hopping and therefore better crystallization. The nature of the two Fe-O layers structure in $LuFe_2O_4$ may require a longer relaxation time than other structure. The comparison of series studies on XRD is shown in Fig.3.16. The growth condition for these pairs experiments was at substrate temperature of 750 ^oC and target composition with Lu：Fe=1：4. One can observe from Fig.3.16 that the coexistence of Lu_2O_3 and $Lu_2Fe_3O_7$ in the film is due to the lack of relaxation time for forming Fe-O layer, therefore low frequency favor the $LuFe_2O_4$ thin film growth.

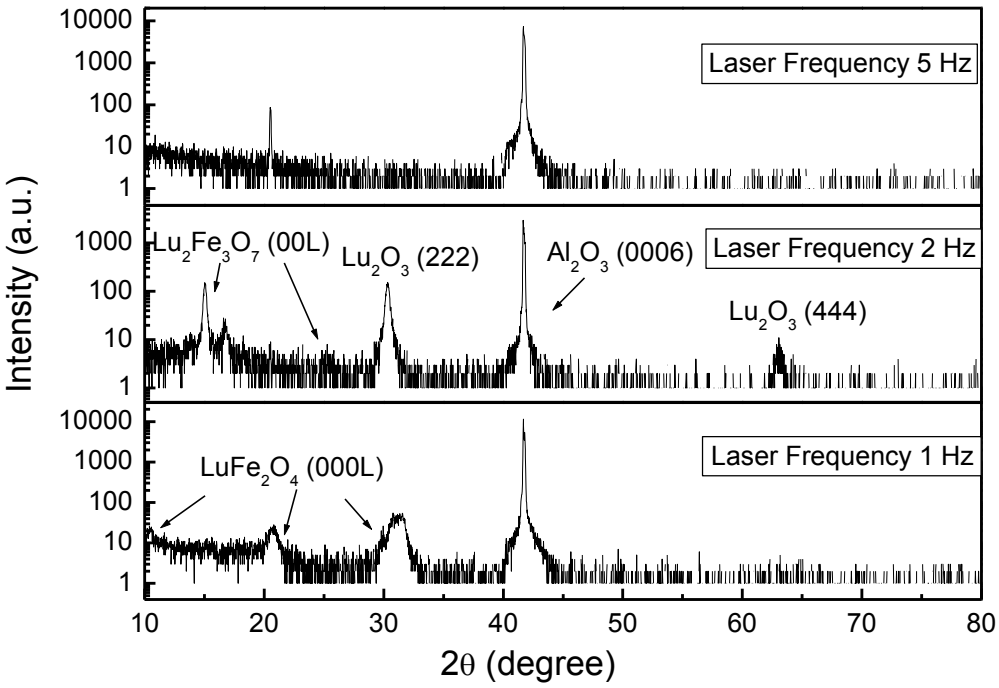

Fig.3.16 XRD patterns of the film deposited with different laser frequencies from 1 Hz to 5 Hz.

3.5 Summary

$LuFe_2O_4$ thin films have been epitaxially deposited on sapphire substrate. Different

growth conditions have been tackled and the growth conditions for $LuFe_2O_4$ film have been optimized. It was found that substrate temperature is the most critical condition for the film growth, where a higher temperature favors the crystallization of the film. 750 ^oC is a critical temperature, below which the film's crystallization is poor and the formation of $LuFe_2O_4$ is difficult. The lower laser frequency favors the formation of better $LuFe_2O_4$ crystallization. The Lu:Fe ratio is also important to form the $LuFe_2O_4$ phase in the film. It is found that higher content of Fe is favorable for the formation of $LuFe_2O_4$ phase, because the interfacial reaction of Fe atoms with Al_2O_3 substrate consumes Fe. However, impurity phase of Fe-O will be induced as the Fe gets over enriched at the end of deposition. Therefore, as the interfacial reaction is unavoidable, a buffer layer is suggested for further deposition.

Chapter 4 Electrical and Magnetic Properties of the $LuFe_2O_4$ Thin Film

4.1 Introduction

$LuFe_2O_4$ bulk material has been demonstrated to possess interesting electrical and magnetic properties such as giant magnetodielectric characteristics, giant dielectric tunability under electrical field. However, these interesting physical properties have never been reported in thin film form $LuFe_2O_4$, since there is no reported successful growth of $LuFe_2O_4$ film so far. In this chapter, characterization results of electrical and magnetic properties of the PLD deposited $LuFe_2O_4$ film, such as dielectric tunability under electric and magnetic fields, as well as temperature-dependent I-V and dielectric characteristics, are reported. Similar trends of dielectric tunability under electric and magnetic fields, as well as non-linear I-V characteristics, are found in the $LuFe_2O_4$ film similar to the bulk. Some phenomena are found for the first time in this material. Magnetic measurement on the $LuFe_2O_4$ thin film was also carried out by means of VSM, where anisotropic magnetic behavior of the film was observed. Magnetic field induced relative permittivity tunability change is also observed in our measurement, indicating a coupling in charge and spin orderings. Since the properties of the $LuFe_2O_4$ film is sample dependent, and the characterizations on other samples were not successful, the result reported in this chapter are all from one sample with best crystallization.

4.2 Electrical Properties of $LuFe_2O_4$

4.2.1 Non-linear current voltage behavior

Current-voltage (I-V) measurement was used to investigate the electrical conductivity

behavior of the $LuFe_2O_4$ film. Although $LuFe_2O_4$ has been reported as an insulator in room temperature, some other studies have shown insulator-to-metal phase transition under electric field. The I-V measurement was carried out by using Keithley 2410 1100V source meter, and the protecting current limitation was set at 0.02 A. The film is 10 nm in thickness, and the inter-digital Au top electrodes have been coated on the surface of the sample with 40 fingers. The width of finger is 10 μm with the gap of 10 μm. The electric field is parallel to the *a*-*b* plane of the $LuFe_2O_4$ film, while the epitaxial growth of the film is along c-axis. A single sweep I-V curve from -3V to 3V is shown in Fig.4.1, where a nonlinear characteristic can be identified. A threshold voltage of 0.5 V can be determined in the measurement. The corresponding threshold electric field is calculated as 500 V/cm, which is an order of magnitude larger than the value (10 V/cm) in bulk $LuFe_2O_4$. [L.J. Zheng, 2009].

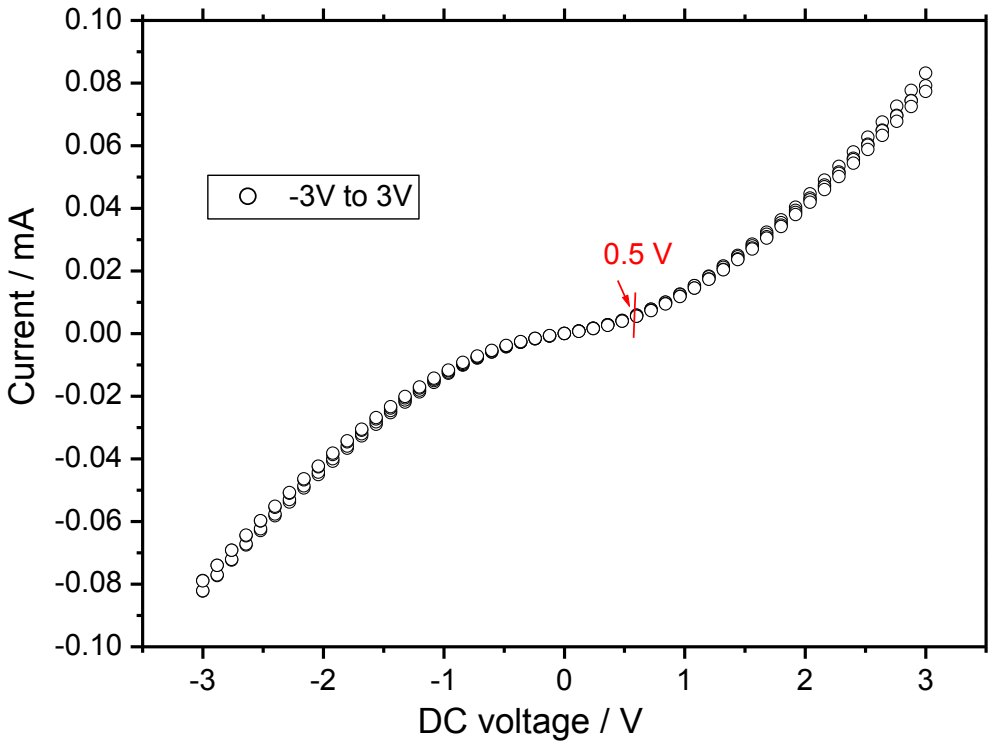

Fig.4.1 A nonlinear I-V curve with sweep voltage from -3V to 3V. A threshold voltage can be determined as 0.5 V.

The combined results are shown in Fig.4.2, in which hysteresis loops can be observed while voltage sweeps. In all the measurements, the resistance of the $LuFe_2O_4$ film decreases with the increasing voltage. This is considered as CO state melting trigged by an electric field. The hysteresis loops become stable after 4 cycles, as show in Fig.4.3.

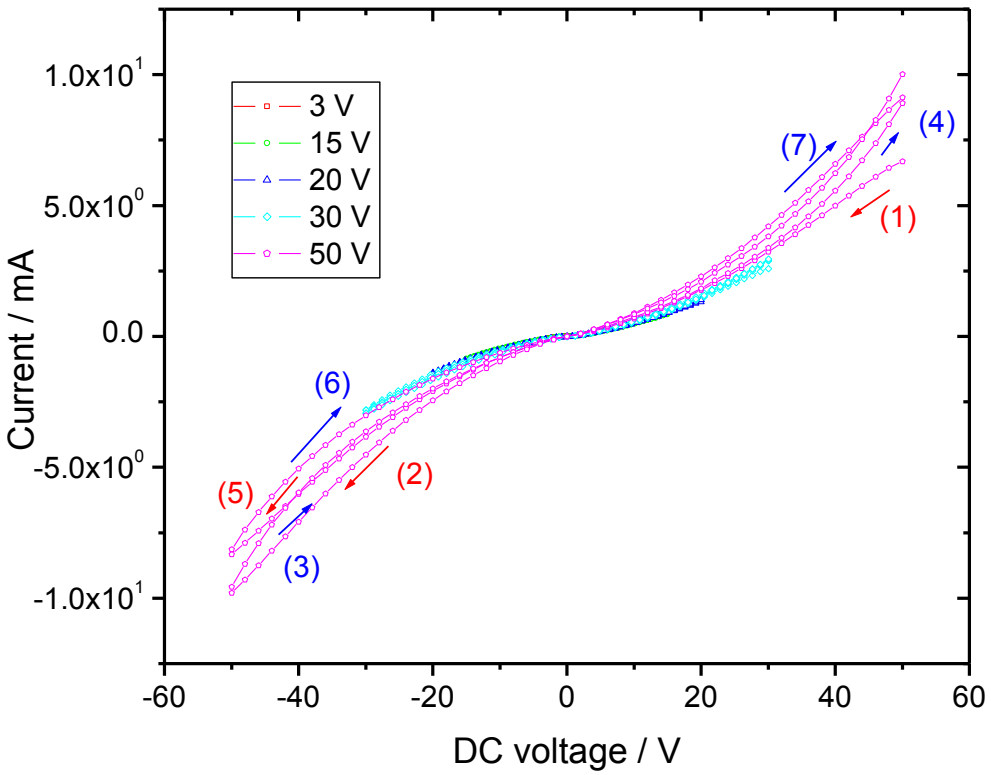

Fig. 4.2 Combined I-V curves of the $LuFe_2O_4$ film with five different dc voltage sweeps.

In $LuFe_2O_4$ single crystal, a resistance switching characteristic induced by applied dc voltage has been reported, suggesting a phase transition induced by electric field. Similar result can sometimes be observed in our $LuFe_2O_4$ film, but the result is not repeatable. The reason is not clear and the result is not shown in the thesis. However, the gradually changed hysteresis in the I-V curves is still consistent with

previous report in the I-V measurement of $LuFe_2O_4$ single crystal, in which the electric field is parallel to the a-b plane [L. J. Zeng, 2008]. Nonlinear I-V characteristic was also reported in the charge-ordered $La_{0.5}Ca_{0.5}MnO_3$ [A. Asamitsu, 1997] and magnetite Fe_3O_4 [S. Lee, A. Fursina, 2008], and several modes have been proposed to interpret the experimental results. However, the transition mechanism is still highly controversial. For instance, a collective transportation of a charge density wave was proposed by Cox et al to interpret this resistance behavior [S. Cox, 2008]. An interpretation of strong Joule heating induced I-V nonlinearity in the regime was proposed by Chen et al [Y. F. Chen, 2007], and has been widely used to explain the resistance switching behavior. However, Zeng *et al* proposed that the CO state breakdown in $LuFe_2O_4$ plays an essential role in the nonlinear I-V behavior. This explanation is supported by their observed appear/disappear of charge ordering with an applied electric filed.

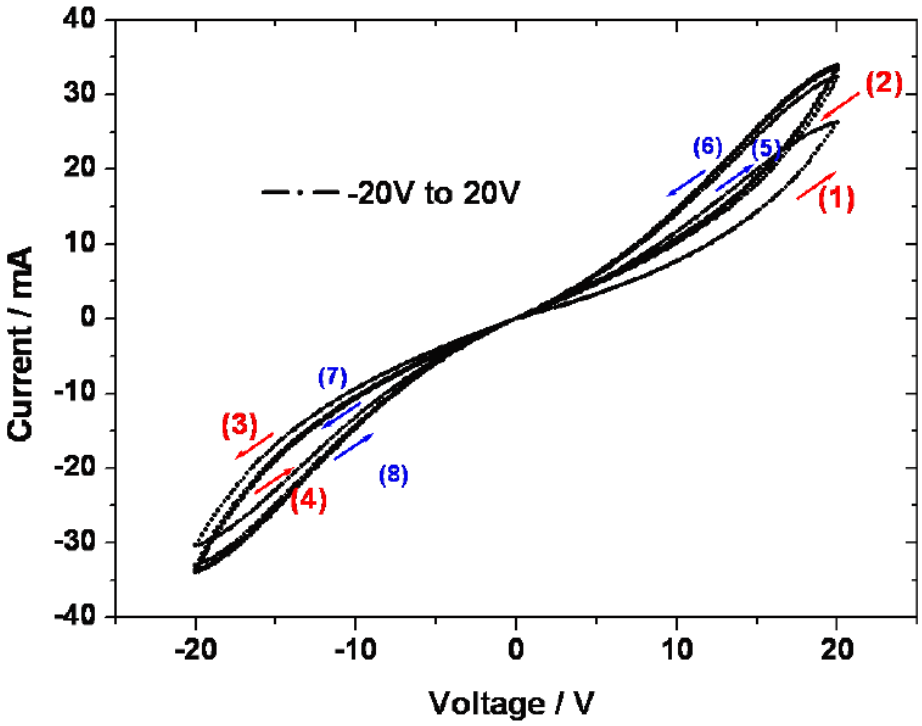

Fig. 4.3 I-V curves of the $LuFe_2O_4$ film with four cycles.

As reported by Zeng *et al*, in $LuFe_2O_4$ bulk material, the charge ordering disappears suddenly after electric field exceeding the threshold voltage. While in our

deposited $LuFe_2O_4$ film, the shift in the hysteresis loop may be caused by the slow CO melting in the film due to the pinning effect of substrate to the domain movement. The hysteresis shift will be eliminated after increasing the time interval of each DC voltage step.

4.2.2 Temperature-dependent resistance characterization

The temperature-dependent resistance of the $LuFe_2O_4$ film with IDT electrodes was measured by using Keithley 6517A high resistance electrometer. The sample was first cooled down to 100 K with a cooling rate of 10 K/min, and then held for 10 min. The measurement was then performed with the output voltage of 10 V, while the sample was warmed up from 100 to 300 K at a heating rate of 10 K/min. In Fig. 4.4, one can observe the relation between resistance and temperature; in general the resistance decreases as the temperature increases. There are two significant resistance changes at 250 K and 340 K, which should correspond to the magnetic transition temperature and charge ordering transition temperature (also known as Curie temperature of $LuFe_2O_4$), respectively. As reported in the literature, the Curie temperature of $LuFe_2O_4$ is defined as the temperature when the charge ordering induced polarization disappears. This experimental result indicates the existence of strong coupling in charge and spin orderings in the $LuFe_2O_4$ film. The discontinuity in the temperature-dependent electrical conductivity at the magnetic transition temperature has also been reported in other RFe_2O_4 family, such as YFe_2O_4 [M. Tanaka 1982] and $ErFe_2O_4$ [J. Iida 1990]. In YFe_2O_4, the mechanism of resistance discontinuity is related to charge ordering, which has been demonstrated by Mössbauer spectroscopy result. The sharp drop in 340 K is caused by insulator-to-metal transition, which has also been reported in previous work [C. H. Li, 2008b]. The resistance change in 340 K shown in Fig.4.4 is not so sharp, which may be due to the impurity phase or imperfect surface

morphology interaction with electrodes, in which total voltage has dropped. This insulator-to-metal phase transition has been reported in other CO state material as mentioned in the last section, and has been thought to be strongly related to CO state transition. In bulk $LuFe_2O_4$, the phase transition at CO temperature is induced by an electric field of 3 V/cm, which is several orders of magnitude smaller than the field in our thin film measurement which is $1x10^4$ V/cm.

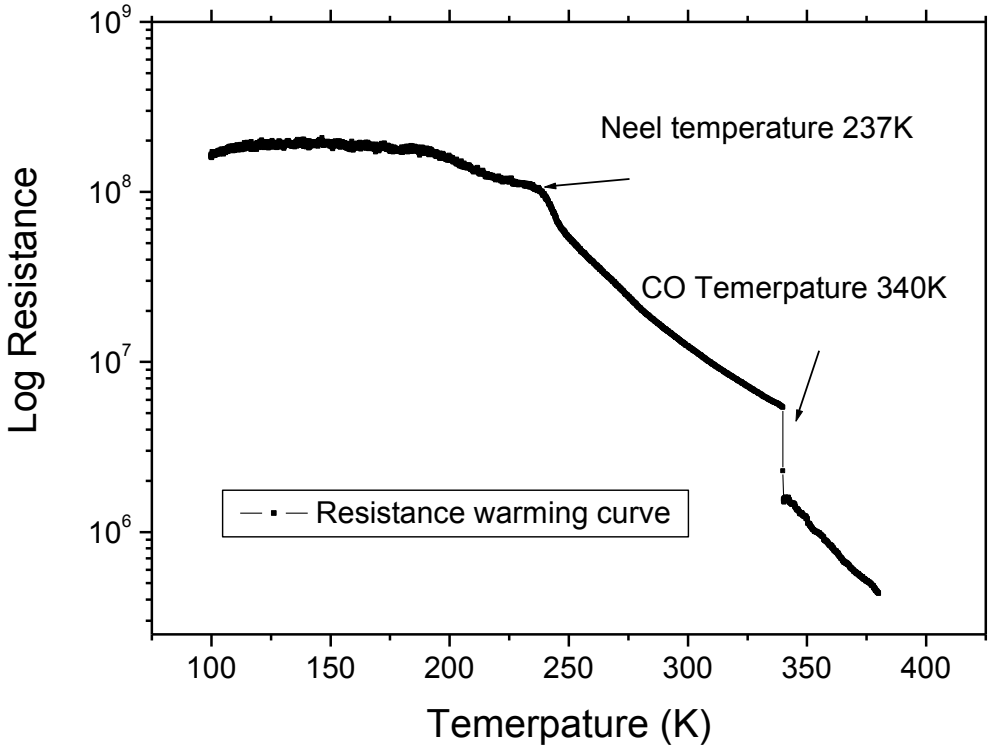

Fig. 4.4 Temperature-dependent resistance curve.

4.2.3 Dielectric tunability at room temperature

Dielectric tunability of the $LuFe_2O_4$ film under electric field was characterized using HP 4294A precision impendent analyzer (frequency range from 1 KHz to 1 MHz) and HP 4291B RF impendent analyzer (frequency range from 1 MHz to 1.8 GHz). The

dielectric measurements were conducted by using C_p-D mode, where C_p represents the capacitance in a parallel circuit model and D represents the loss tangent. The details of calibration in HP 4291B are introduced in Chapter 2. The finger spacing of IDT electrode is 10 μm and finger width is also 10 μm.

Frequency-dependent dielectric constant and loss of the $LuFe_2O_4$ film are plotted in Fig. 4.5, where the dielectric constant of the $LuFe_2O_4$ film is extremely large and decreases as frequency increases. Although the large dielectric constant in $LuFe_2O_4$ is a common feature of RFe_2O_4 family (normally in the order of 10^4), the extremely large dielectric constant of the $LuFe_2O_4$ film at low frequency regime is believed to be contributed by the relatively large leakage current of the film. This is in consistent with the large dielectric loss at low frequency.

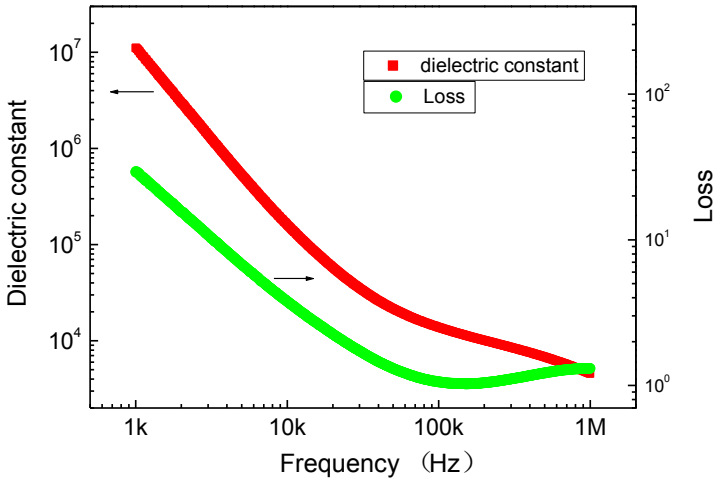

Fig. 4.5 Spectroscopic dielectric constant (real and imaginary parts).

Figure 4.6 shows the dielectric tunability of the $LuFe_2O_4$ film under dc bias voltage. It is apparent that the dielectric constant decreases with the increase of bias voltage, and the loss tangent increases with the increase of bias voltage. All the measurements were performed at room temperature and the ac amplitude was set to

0.5 V. A dielectric tunability of 10 % at ±5 V can be observed in the 1 MHz measurement, which is relatively small compared to the value found in bulk $LuFe_2O_4$.[C.H. Li, 2008a]

The dielectric tunability plotted is defined as follow:

$$N = \frac{\varepsilon(E)-\varepsilon(0)}{\varepsilon(0)}, \quad (4.1)$$

where N is the tunability ratio representing the decrease in relative permittivity. ε(E) is the relative permittivity under electric field E, and ε(0) is the relative permittivity without external electric field.

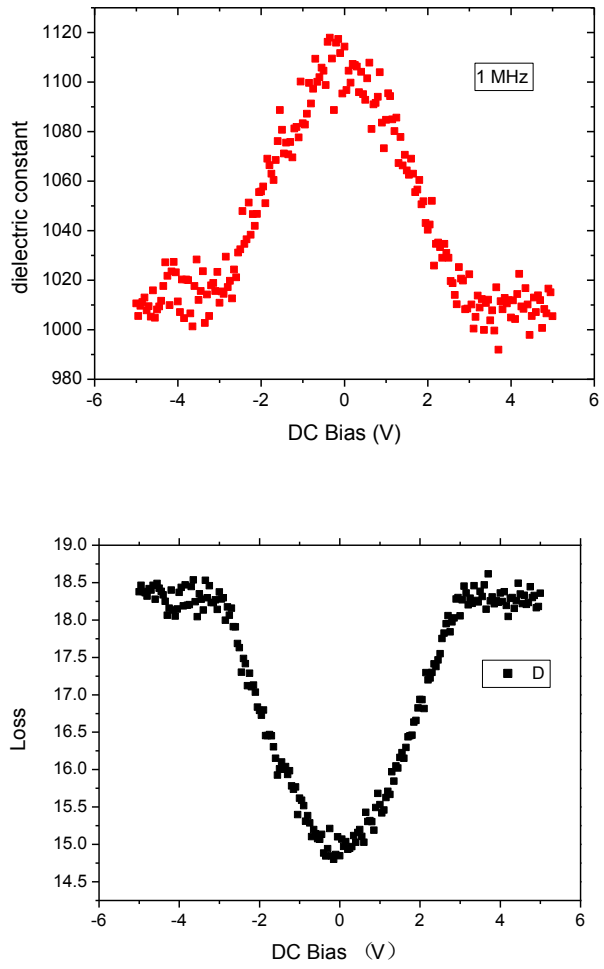

Fig. 4.6 C-V curves and dielectric loss of the $LuFe_2O_4$ film measured on HP 4291B at

frequency of 1 MHz with DC bias voltages swept from -5 to 5 V.

Figure 4.7 is the tunability-voltage (*K*-*V*) curves of the $LuFe_2O_4$ film at different frequencies. Charge ordering induced polarization in $LuFe_2O_4$ is believed to be responsible for the large dielectric constant, and electric filed breaks the charge ordering in $LuFe_2O_4$ and reduces the ferroelectricity, and thus reduces the dielectric constant. This is believed to be the origin of the dielectric tunability in $LuFe_2O_4$. Giant dielectric tunability of $LuFe_2O_4$ ceramic has been reported earlier at frequencies below 200 kHz [C. H. Li, 2008(a)], but the tunability at high frequency and microwave range is unknown. In our $LuFe_2O_4$ film, it is found that the dielectric tunability decreases as the frequency increases and eventually disappears when the testing frequency is higher than 500 MHz. The physics behind this frequency-dependent tunability needs further study.

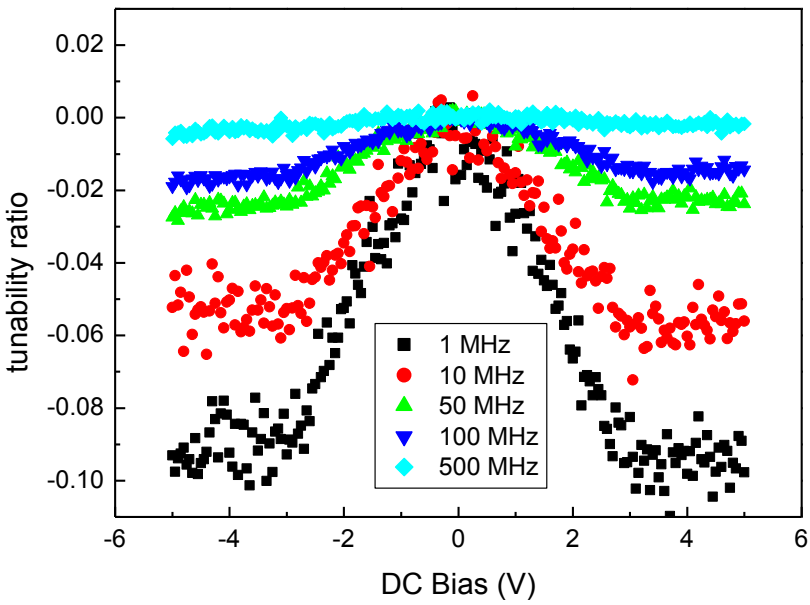

Fig. 4.6 Frequency-dependent dielectric tunability of the $LuFe_2O_4$ film.

4.2.4 Temperature-dependent dielectric properties

Temperature-dependent dielectric measurement of the $LuFe_2O_4$ film with IDT electrode was done with HP 4291A impendent analyzer. The sample was first cooled by liquid nitrogen to 77 K, held for 15 min, and then warmed up to 370 K with a rate at 1^oC /min. The measurement result is plotted in Fig.4.8 from 1 kHz to 100 kHz. One can see a relatively large capacitance at low frequency, while the unexpected high capacitance (the value is one order of magnitude larger than the bulk sample) is due to the high leakage current at low frequency. However one can still see the influence of temperature to the trend of dielectric constant. The similar curve from 180 K to 230 K in both capacitance and loss can be explained by the large leakage current contributed result. As shown in Fig. 4.8 (a), the step in capacitance at 130 K is believed to be related to the Verwey transition of Fe_3O_4 impurity phase formed in the film due to the Fe-enriched target. The peak of the imaginary part of dielectric constant at low frequency indicates a significant change in mechanism of polarization, which may be caused transition from 3-D charge ordering to 2-D charge ordering.

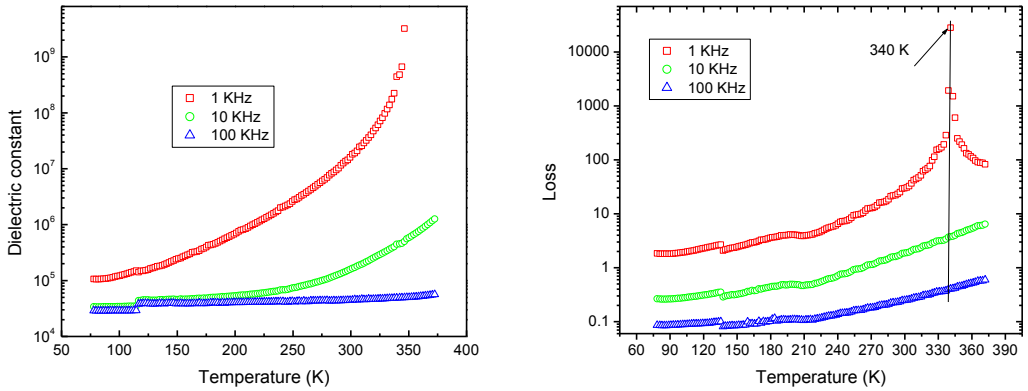

Fig. 4.8 Temperature-dependent dielectric constant (a), and loss (b), of the $LuFe_2O_4$ film at different frequencies.

There is a peak at 340 K in both dielectric constant and loss measured at 1 KHz,

as shown in Fig.4.9. This can be explained by the charge ordering transition at this temperature. Electric field induced insulator-to-metal transition is believe to explain this kind of change in previous work [C.H. Li, 2008], and the sharp drop in resistance can also be observed in our temperature-dependent resistance measurement. In Fig. 4.9, the capacitance at 1 KHz changes to negative at a transition temperature of 340 K, suggesting metal behavior of the film beyond 340 K, the CO temperature. It is worth noting that this change only presents in the low frequency measurement. This phenomenon is consistent with our results in temperature-dependent resistance change in 340 K. The sharp change in resistance shows an insulator-to-metal transition at 340 K, which also affects the value in dielectric constant.

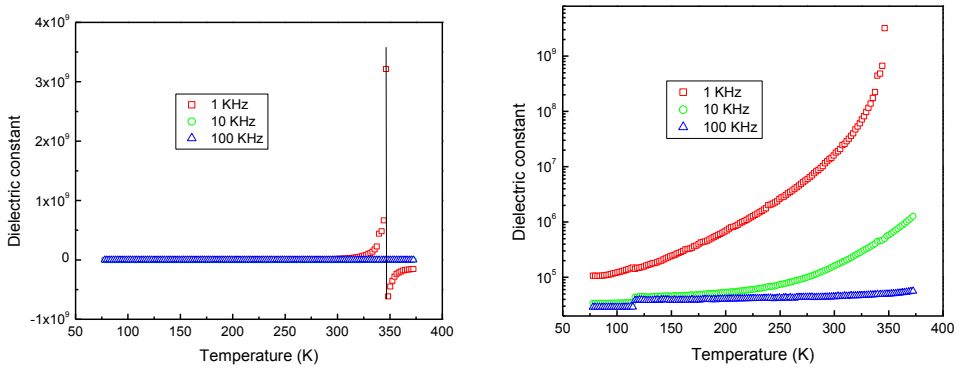

Fig. 4.9 dielectric constant-temperature curve of the $LuFe_2O_4$ film, in which a peak has been observed at 340 K. The left image is plot in linear scale and the right one is plot in log scale.

4.3 Magnetic properties of $LuFe_2O_4$

Magnetization measurements have been carried out at room temperature on two samples by using VSM. The first sample is deposited by Lu:Fe=1:4 target, and the measurement result is shown in Figs.4.10 and 4.11; while the second sample is deposited by a target with Lu:Fe=1:2, and the result is shown in Figs.4.12 and 4.13. The external magnetic field was applied along c axis and a-b plane, respectively, and

the anisotropic magnetization is apparent. The measurement was carried out under -2500 Oe to 2500 Oe in Fig. 4.10, and -1500 Oe to1500 Oe in Fig. 4.11.

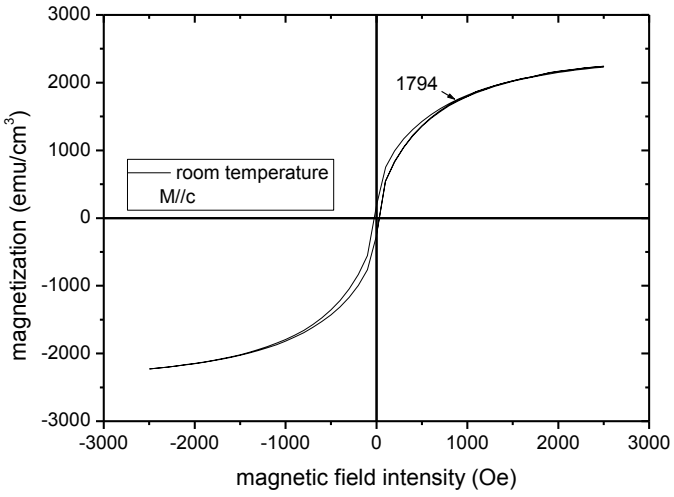

Fig.4.10 M-H hysteresis loop of the film deposited by the Lu:Fe=1:4 target. The magnetic field is parallel to c axis.

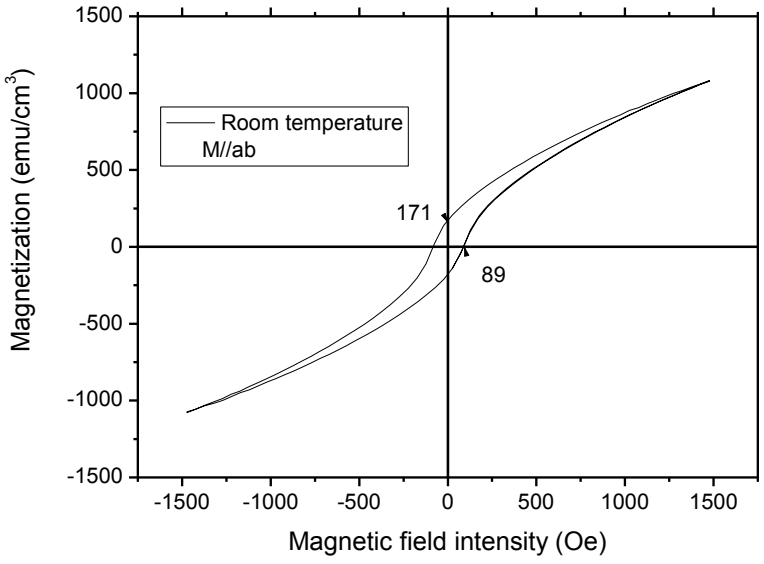

Fig. 4.11 M-H hysteresis loop of the sample deposited by the Lu:Fe=1:4 target. The magnetic field is parallel to a-b plane.

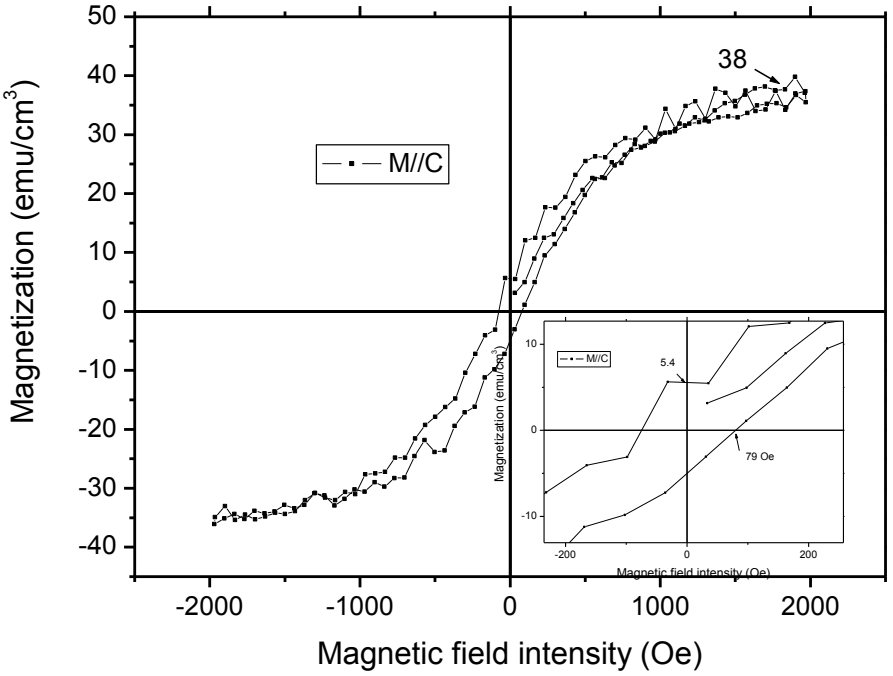

Fig.4.12 M-H hysteresis loop of the sample deposited by the Lu:Fe=1:2 target. The magnetic field is parallel to c axis. The inset picture is magnified at the origin.

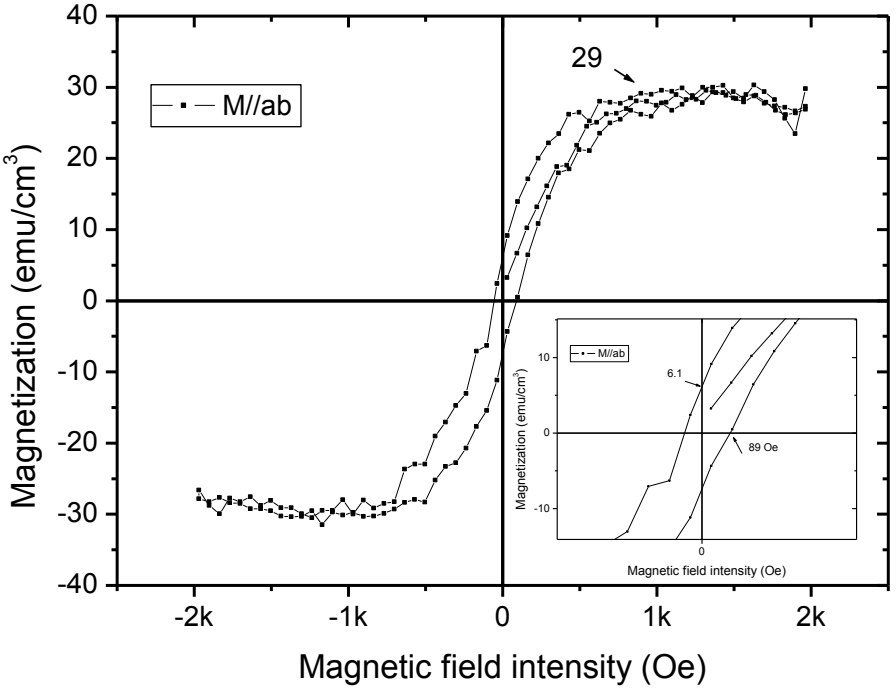

Fig.4.13 M-H hysteresis loop of the sample deposited by the Lu:Fe=1:2 target. The

magnetic field is parallel to a-b plane. The inset picture is magnified at the origin.

In Fig.4.12, the saturation magnetization is 29 emu/cm^3 at 2000 Oe when the external field is parallel to *a*-*b* plane; while in Fig. 4.13, the saturation magnetization is 38 at 1000 Oe when the external field is parallel to *c* axis. The magnetization is relatively larger when the external field is parallel to *c* axis, suggesting that the spin of Fe ions is parallel to *c* axis. The coercive field in Fig. 4.12 is 89 Oe, and the coercive field in Fig. 4.13 is 79 Oe, meaning that the magnetic order in the $LuFe_2O_4$ thin film is softer along *c* axis. It should be noticed that these results are all suffered from noise, because VSM is not quite suitable for measuring small sample such as thin films. Though $LuFe_2O_4$ is supposed to have ferromagnetic behavior only under 240 K, the M-H hysteresis loops at room temperature were also report at $LuFe_2O_4$ polycrystalline pelletized sample. [J.Y. Park, 2007]

By comparing the results from these two samples, one can conclude that the magnetization in sample one is two orders of magnitude larger than that of sample two. The difference between the magnetization behavior is believed to be due to the contribution of Fe_3O_4 impurity phase in the sample deposited by iron-enriched target (Lu:Fe=1:4). Therefore our analysis has been focused on sample two, as it reveals the $LuFe_2O_4$ magnetic properties in the film.

4.4 Electrical and Magnetic Coupling

Relative permittivity characterization under both magnetic and electric fields was performed on $LuFe_2O_4$ thin film by using C_p-D mode in 4294A impendence analyzer. Static magnetic field was applied by electro-magnet of 0.83 T, and electrical voltage was swept from -5 to 5 V. Figure 4.14 shows measurement result of the electric and magnetic field-dependent dielectric tunability. It is apparent that the tunability triggered by DC bias under magnetic field is smaller than that without magnetic field.

One can see that the dielectric tunability without magnetic field at ±5 V is 35%, but decreases to 20% with 0.83 T magnetic field applied paralleled to the *a*-*b* plane of the film, and further decreases to 15% with same magnetic field applied paralleled to the *c* axis of the film. The loss tangent also decreases under magnetic field in $LuFe_2O_4$ film as shown in Fig. 4.16.

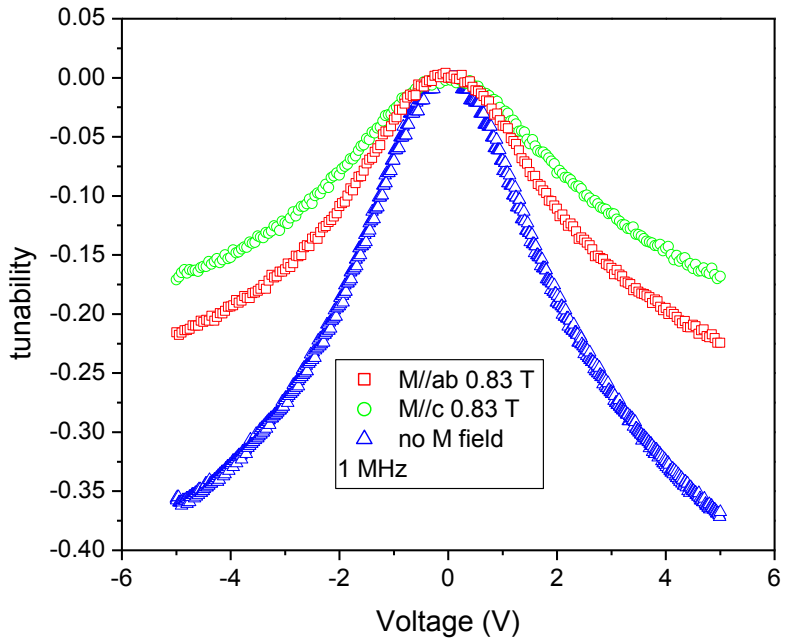

Fig. 4.14 Measurement result of the electric and magnetic field-dependent dielectric tunability with magnetic field applied on different directions.

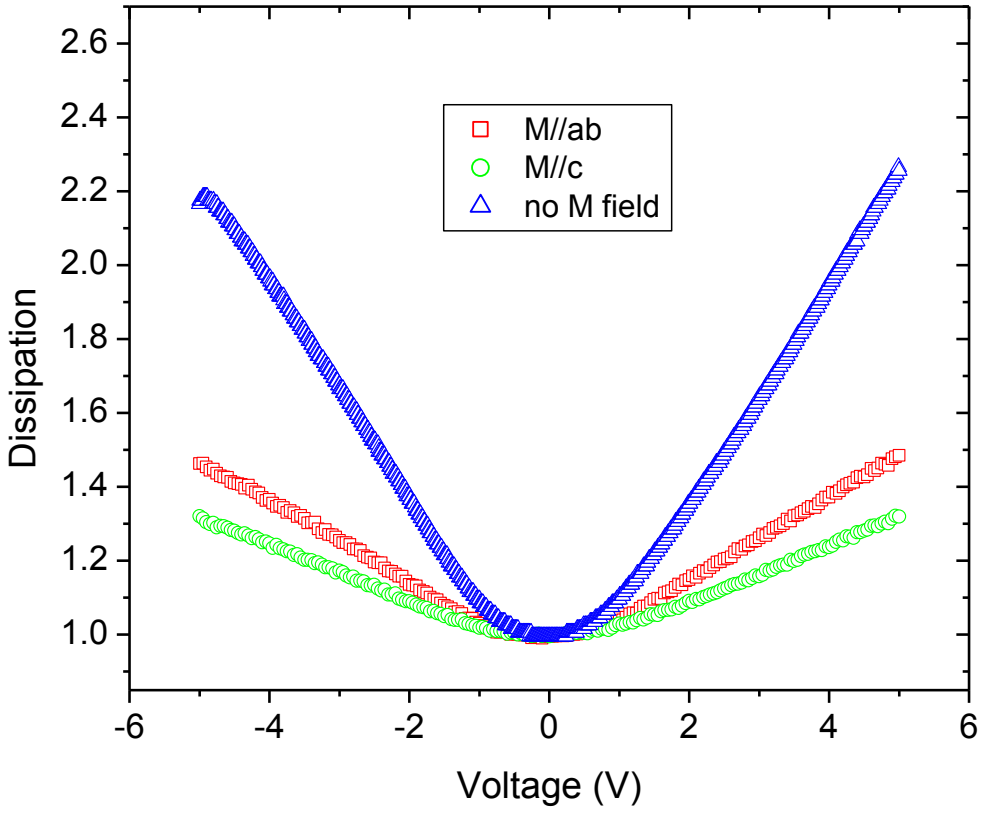

Fig.4.15 Dielectric dissipation of the film under both electric field and magnetic field at different directions.

As the electric polarization is induced by the charged ordering of Fe *3d* charge states in $LuFe_2O_4$, which also contribute to the magnetic spin arrangement in this material, the spin and charge orderings should have strong correlation. [A. Nagano, 2007] Yet the nature of CO sequence and transition between CO state are controversial. It is generally believed that the magnetic field alternates the arrangement of Fe^{2+} and Fe^{3+} ions, therefore changes the CO states of $LuFe_2O_4$. [H. J. Xiang, 2007] The physics behind this phenomenon is that the tunability under DC bias is due to CO melting in the $LuFe_2O_4$,[C. H. Li, 2008 (a)] but the magnetic field may pinning the spin arrangement of 3*d* electrons in Fe ions, leading to an increased threshold energy for the CO melting and therefore reduces the tunability under DC

bias in $LuFe_2O_4$.

4.5 Summary

Nonlinear I-V behavior of the $LuFe_2O_4$ thin film has been observed and threshold voltage is found to be larger than that of bulk $LuFe_2O_4$. Electric field induced phase transition is observed at the CO transition temperature and Neel temperature of the $LuFe_2O_4$ film under 10 V. The CO breakdown voltage of the film is also found to be higher than that of bulk $LuFe_2O_4$, which may be due to the pinning effect of grain boundaries in the film or by substrate.

Dielectric tunability is also observed in the $LuFe_2O_4$ film, with saturation voltage of 2.5 V. The tunability decreases with increasing frequency, and finally vanishes at 500 MHz. The temperature-dependent dielectric behavior is also characterized and an insulator-to-metal phase transition is observed at 340 K.

Dielectric tunability under both magnetic and electric fields is found. The magnetic field increases the required electric field to break the charge ordering in the $LuFe_2O_4$ film, therefore decreases the film's dielectric tunability under electric field.

Chapter 5 Conclusions and future work

In this thesis the growth and characterization of $LuFe_2O_4$ thin films have been studied and the following results have been achieved.

$LuFe_2O_4$ thin films (with thicknesses in the range of around 100 nm) have been fabricated by pulsed-laser deposition on (0001) Al_2O_3 substrate and the microstructure of the $LuFe_2O_4$ films have been studied by means of x-ray diffraction and transmission electron microscopy. Different deposition conditions have been used in order to optimize the condition for the $LuFe_2O_4$ film growth. Finally, the $LuFe_2O_4$ film is successively grown on the (0001) sapphire substrate, and it is found that the critical temperature to synthesis the $LuFe_2O_4$ film is above 750^oC; while the higher the temperature of substrate in deposition the better the crystallization. It is also found that oxygen pressure in the deposition and annealing is critical to electrical and magnetic properties of the films, suggesting that the ratio of Fe^{2+} and Fe^{3+} in the film is sensitive to oxygen pressure. In addition, Fe-enriched target is found to be favorable in forming the $LuFe_2O_4$ film, and the interfacial reaction is responsible for this phenomenon. It is believed that the interfacial reaction happens at the earlier stage of $LuFe_2O_4$ film growth under high temperature, during which Fe atoms diffuse into the Al_2O_3 substrate resulting in the formation of $FeAl_2O_4$ interfacial reaction phase. Fe-enriched target provides a right ratio of Fe:Lu after some Fe is consumed. However, impurity phase of Fe-O, such as Fe_2O_3 and Fe_3O_4, may be formed as the Fe element becomes enriched in the subsequent deposition.

Detailed studies have also been carried out to investigate the electrical and magnetic properties of the $LuFe_2O_4$ thin films. Gold inter digital electrodes are coated on the $LuFe_2O_4$ film surface for the electrical characterization. A large dielectric tunability under electric field is revealed in the film; while the dielectric tunability

decreases as the frequency increases, and eventually the dielectric tunability disappears above 500 MHz. Electric field induced phase transition is believed to be responsible for the dielectric tunability in the $LuFe_2O_4$ film, in which the applied electric filed breaks the charge ordering in the $LuFe_2O_4$ system and reduces the dielectric permittivity. Temperature-dependent phase transition is revealed in both dielectric and resistance measurements, where near the charge ordering transition temperature the $LuFe_2O_4$ film experiences an insulator-to-metal transition due to the charge ordering breakdown. Magnetic properties have also been studied by means of vibrating sample magnetometer measurement, where anisotropic magnetic properties of the $LuFe_2O_4$ film are found. Magnetodielectric coupling in the $LuFe_2O_4$ film has been found in dielectric measurement under both DC bias and magnetic field, and a decrease of the dielectric tunability under DC bias has been observed when a small magnetic field was applied.

However, due the limitation of time, there are still some issues have not been addressed. For example, even the $LuFe_2O_4$ films have been successfully deposited, the growth mechanism is not fully understood yet. More work can be done to deeply study the growth mechanism and the interfacial reaction at different growth conditions. The ratios of Fe^{2+}:Fe^{3+} in the different films grown at different oxygen pressures also deserve further study.

Some very interesting phenomena have been observed in this thesis work, however, more work need to be done to study the relationship between the different physical properties and the structure of the films.

Reference

A. Chen, F. Chernow, (1967). "Nature of Ferroelectricity in KNO_3." Phys. Rev. **154**(2): 493 - 505

A. Feteira, D. C. Sinclair, I. M. Reaney, Y. Somiya, and M. T. Lanagan, (2004). "$BaTiO_3$-Based Ceramics for Tunable Microwave Applications." J. Am. Ceram. Soc. **87**(6): 1082.

A. M. Mulders, S. M. Lawrence, U. Staub, M. Garcia-Fernandez, V. Scagnoli,4 C. Mazzoli, E. Pomjakushina, K. Conder, and Y. Wang (2009). "Direct Observation of Charge Order and an Orbital Glass State in Multiferroic $LuFe_2O_4$." Phys. Rev. Lett. **103**(7): 077602.

A. Moreira dos Santosa, S. Parasharb, A. R. Rajub, Y. S. Zhaoc, A. K. Cheethama, 1 and C. N. R. Rao (2002). "Evidence for the likely occurrence of magnetoferroelectricity in the simple perovskite, $BiMnO_3$ " Solid State Commun. **122**(1-2): 49-52.

A. Nagano, M. Naka, J. Nasu, and S. Ishihara, (2007). "Electric Polarization, Magnetoelectric Effect, and Orbital State of a Layered Iron Oxide with Frustrated Geometry." Phys. Rev. Lett. **99**(21): 217202.

A. P. Levanyuk, D. G. Sannikov (1974). " Improper ferroelectrics." Sov. Phys. Usp. **17**(2): 199-214

A.D. Christianson, M. D. Lumsden, M. Angst, Z. Yamani, W. Tian, R. Jin, E. A. Payzant, S. E. Nagler, B. C. Sales, and D. Mandrus (2008). "Three-Dimensional Magnetic Correlations in Multiferroic $LuFe_2O_4$ " Phys. Rev. Lett. **100**: 107601.

C. G. Zhong, Q. Jiang (2002). "The study of the coupling mechanism between antiferromagnetic and ferroelectric ordering and thermodynamic properties in ferroelectromagnets." J. Phys. Condens. Matter **14**: 8605.

C. H. Li, X. Q. Zhang, Z. H. Cheng, and Y. Sun (2008). "Electric field induced phase transition in charge-ordered $LuFe_2O_4$." Appl. Phys. Lett. **93**(15): 152103.

C. H. Li, X. Q. Zhang, Z. H. Cheng, and Y. Sun, (2008). "Room temperature giant dielectric tunability effect in bulk $LuFe_2O_4$." Appl. Phys. Lett. **92**(18): 182903.

C. H. Li, F. Wang, Y. Liu, X. Q. Zhang, Z. H. Cheng, and Y. Sun, (2009). "Electrical control of magnetization in charge-ordered multiferroic $LuFe_2O_4$." Phys. Rev. B **79**(17): 172412.

Chen, L.-C. (1994). "Particulates generated by pulsed laser deposition", John Wiley & Sons.

D. Ito, N. Fujimura, and T. Ito (2000). "Initial Stage of Film Growth of Pulsed Laser Deposited $YMnO_3$." Japan. J. Appl. Phys. **39**: 5525.

D. Ito, N. Fujimura, T. Yoshimura, and T. Ito (2003). "Influence of Schottky and Poole–Frenkel emission on the retention property of $YMnO_3$-based metal/ferroelectric/insulator/semiconductor capacitors." J. Appl. Phys. **94**(6): 4036.

D. L. Fox, D. R. Tilley, J. F. Scott, H. J. Guggenheim, (1980). "Magnetoelectric phenomena in $BaMnF_4$ and $BaMn_{0.99}Co_{0.01}F_4$." Phys. Rev. B **21**(7): 2926.

D. P. Norton (2007). “Complex oxide film growth”, Wiley-Interscience.

D.I. Khomskii (2008). "Multiferroics: Different ways to combine magnetismand ferroelectricity." Journal of Magnetism and Magnetic Materials **306**: 1-8.

E. Ascher, H. Rieder, H. Schmid, H. Sto ̈ssel (1966). "Some Properties of Ferromagnetoelectric Nickel-Iodine Boracite, $Ni_3B_7O_{13}I$." J. Appl. Phys. **37**(3): 1404.

E. Hanamura, K. Hagita & Y. Tanabe (2003). "Clamping of ferroelectric and antiferromagnetic order parameters of $YMnO_3$." J. Phys. Condens. Matter **14:** 103.

G. A. Smolenskii, V. A. Bokov, B. A. Isupov, N. N. Krainik, R. E. Pasynkov, M. S. Shur (1971). Ferroelectrics and Antiferroelectrics. Leningrad, Nauka Publishers.

G. Catalan (2006). "Magnetocapacitance without magnetoelectric coupling." Appl. Phys. Lett. **88**(10): 102902.

G. Gorodetsky, R. M. Hornreich, B. M. Wanklyn, (1973). "Statistical Mechanics and Critical Behavior of the Magnetoelectric Effect in $GdVO_4$." Phys. Rev. B **8**(5): 2263.

G. K. Hubler (1994). “Comparison of vacuum deposition techniques”, John Wiley & Sons.

G. Lawes, A. B. Harris, T. Kimura, N. Rogado, R. J. Cava, A. Aharony, O. Entin-Wohlman, T. Yildirim, M. Kenzelmann, C. Broholm, and A. P. Ramirez. (2005). "Magnetically Driven Ferroelectric Order in $Ni_3V_2O_8$." Phys. Rev. Lett. **95**(8): 087205.

G. T. Rado (1969). "Magnetoelectric Evidence for the Attainability of Time-Reversed Antiferromagnetic Configurations by Metamagnetic Transitions in $DyPO_4$." Phys. Rev. Lett. **23**(12): 644.

G.A. Smolenskii, I.E. Chupis (1982). "Ferroelectromagnets." Sov. Phys. Usp **475**(25).

H. Hanafi, S. Tiwari, and I. Khan, (1996). "Fast and long retention-time nano-crystal memory." IEEE Trans. Electron Devices **43**: 1553.

H. J. Xiang and M. H. Whangbo (2007). "Charge Order and the Origin of Giant Magnetocapacitance in $LuFe_2O_4$." Phys. Rev. Lett. **98**: 246403.

H. N. Lee, Y. T. Kim, and Y. K. Park (1999). "Memory window of highly c-axis oriented ferroelectric $YMnO_3$ thin films." Appl. Phys. Lett. **74**(25): 3887

H. Schmid (1994). "Introduction to the proceedings of the 2nd international conference on magnetoelectric interaction phenomena in crystals, MEIPIC-2." Ferroelectrics **161**: 1-28.

J. Dho, C. W. Leung, J. L. MacManus-Driscoll and M. G. Blamire (2004). "Epitaxial and oriented $YMnO_3$ film growth by pulsed laser deposition " J. Cryst. Growth **267**: 548.

J. Iida, M. Tanaka, Y. Nakagawa, S. Funahashi, N. Kimizuka and S. Takekawa, (1993). "Magnetization and Spin Correlation of Two-Dimensional Triangular Antiferromagnet $LuFe_2O_4$." J. Phys. Soc. Jpn. **62**: 1723.

J. P. Rivera (1994). "On definition, units, measurements, tensor forms of the linear

magnetoelectric effect and on a new dynamic method applied to Cr-Cl boracite. ." Ferroelectrics **161**: 165-180.

J. S. Horwitz, and J. A. Aprague, (1994). “Film nucleation and film growth in pulsed laser deposition of ceramics”, John Wiley & Sons.

J. Wang, J. B. Neaton, H. Zheng, V. Nagarajan, S. B. Ogale, B. Liu, D. Viehland, V. Vaithyanathan, D. G. Schlom, U. V. Waghmare, N. A. Spaldin, K. M. Rabe, M. Wuttig, R. Ramesh (2003). "Epitaxial $BiFeO_3$ Multiferroic Thin Film Heterostructures." Science **299**: 1719.

J.Y. Park, J. H. Park, Y. K. Jeong, and H. M. Janga, (2007). "Dynamic magnetoelectric coupling in “electronic ferroelectric” $LuFe_2O_4$." Appl. Phys. Lett. **91**(15): 152903.

K. M. Johnson (1962). "Variation of Dielectric Constant with Voltage in Ferroelectrics and Its Application to Parametric Devices." J. Appl. Phys. **33**(9): 2826.

K. S. Sree Harsha (2006). "Principles of Physical Vapor Deposition of Thin Films." Pergamon Press

K. Siratori, S. Funahashi, J. Iida, and M. Tanaka, (1992). Ferrites, Proc. 6th Int. Conf. on Ferrites Tokyo and Kyoto, The Japan Society of Powder and Powder Metallurgy.

K. Y. Yun, M. Noda , M. Okuyama, H. Saeki, H. Tabata and K. Saito, (2004). "Structural and multiferroic properties of $BiFeO_3$ thin films at room temperature." J. Appl. Phys. **96**(6): 3399.

K. Yoshii, N. Ikeda, Y. Matsuo, Y. Horibe, and S. Mori, (2007). "Magnetic and

dielectric properties of RFe_2O_4, $RFeMO_4$, and $RGaCuO_4$ (R=Yb and Lu, M=Co and Cu)." Phys. Rev. B **76**(2): 024423.

M. A. Saifi, L. E. Cross, (1970). "Dielectric properties of strontium titanate at low temperatures." Phys. Rev. B **2**: 677-684.

M. A. Subramanian, T. He, J. Z. Chen, N. S. Rogado, T. G. Calvarese, and A. W. Sleight, (2006). "Giant Room–Temperature Magnetodielectric Response in the Electronic Ferroelectric $LuFe_2O_4$." Adv. Mater. **18**: 1737.

M. Angst, R. P. Hermann, A. D. Christianson, M. D. Lumsden, C. Lee, M.-H. Whangbo, J.-W. Kim, P. J. Ryan, S. E. Nagler, W. Tian, R. Jin, B. C. Sales, and D. Mandrus, (2008). "Charge Order in $LuFe_2O_4$: Antiferroelectric Ground State and Coupling to Magnetism." Phys. Rev. Lett. **101**(22): 227601.

M. Fiebig, Th. Lottermoser, D. Fro ̈hlich, A. V. Goltsev, & R. V. Pisarev (2002). "Observation of coupled magnetic and electric domains." Nature **419**: 818–820.

M. G. Norton, and C. B. Carter, (1990). "On the optimization of the laser ablation process for the deposition of $YBa_2Cu_3O_7$-Delta thin films." Physics C **172**: 47.

M. Isobe, N. Kimizuka, J. Iida and S. Takekawa (1990). "Structures of $LuFeCoO_4$ and $LuFe_20_4$." Acta Cryst. C**46**: 1917-1918.

M. Kenzelmann, A. B. Harris, S. Jonas, C. Broholm, J. Schefer, S. B. Kim, C. L. Zhang, S.-W. Cheong, O. P. Vajk, J.W. Lynn (2005). "Magnetic Inversion Symmetry Breaking and Ferroelectricity in $TbMnO_3$." Phys. Rev. Lett. **95**(8): 087206.

M. Mostovoy (2006). "Ferroelectricity in Spiral Magnets." Phys. Rev. Lett. **96**(6): 067601.

M. Naka, A. Nagano, and S. Ishihara (2008). "Magnetodielectric phenomena in a charge- and spin-frustrated system of layered iron oxide." Phys. Rev. B **77**(22): 224441.

M. Ohring (1991). Materials Science of Thin Film -Deposition and structure, New York, Academic Press.

M. Tanaka, H. Iwasaki, K. Siratori, and I. Shindo, (1989). "Mössbauer Study on the Magnetic Stracture of $YbFe_2O_4$: A Two-Dimensional Antiferromagnet on a Triangular Lattice." J. Phys. Soc. Jpn. **58**: 1433.

N. A. Hill (2000). "Why are there so few magnetic ferroelectrics?" J. Phys. Chem. B **104**: 6694-6709.

N. Fujimura, T. Ishida, T. Yoshimura, and T. Ito (1996). "Epitaxially grown $YMnO_3$ film: New candidate for nonvolatile memory devices." Appl. Phys. Lett. **69**(7): 1011.

N. Hur, S. Park, P. A. Sharma, J. S. Ahn, S. Guha and S-W. Cheong (2004). "Electric polarization reversal and memory in a multiferroic material induced by magnetic fields." Nature **429**(392).

N. Ikeda, S. Mori, K. Kohn, (2005). "Charge Ordering and Dielectric Dispersion in Mixed Valence Oxides RFe_2O_4." Ferroelectrics **314**: 41–56.

N. Ikeda, H. Ohsumi, K. Ohwada, K. Ishii, T. Inami, K. Kakurai, and K. Y. Y.

Murakami, S. Mori, Y. Horibe & H. Kito (2005). "Ferroelectricity from iron valence ordering in the charge-frustrated system $LuFe_2O_4$." Nature **436**(25): 04039.

N. Iwata, K. Kohn (1998). "Dielectric anomalies at magnetic transitions of hexagonal rare earth manganese oxides $RMnO_3$." J. Phys. Soc. Jpn **67**: 3318–3319.

N. Kimizuka, E. Muromachi and K. Siratori (1990). Handbook on the Physics and Chemistry of Rare Earths. North-Holland, Elsevier Sci. Press.

N. Kimizuka, E. Muromachi, & K. Siratori, (1990). Handbook on the Physics and Chemistry of Rare Earths. Amsterdam, Elsevier Science.

R. E. Cohen (2000). "Theory of ferroelectrics: a vision for the next decade and beyond." J. Phys. Chem. Solids **61**: 139-146.

R. Seshadri, N.A. Hill (2001). "Visualizing the role of Bi *6s* “lone pairs” in the off-center distortion in ferromagnetic $BiMnO_3$." Chem. Mater **13**(9): 2892.

S. Funahashi, J. Akimitsu, K. Siratori, N. Kimizuka, M. Tanaka and H. Fujishita (1984). "Two-Dimensional Spin Correlation in YFe_2O_4." J. Phys. Soc. Jpn. **53**: 2688.

S. Metev, and M. Sendova, Trends in Quantum Electronic. Bellingham, SPIE.

S. Metev (1994). “Process characteristics and film properties in pulsed laser deposition”. John Wiley & Sons,.

S. Nakamuraa, H. Kito, M. Tanaka, (1998). "An approach to specify the spin configuration in the RFe_2O_4 (R=Y, Ho, Er, Tm, Yb, and Lu) family: Fe Mössbauer

study on a single crystal $LuFe_2O_4$." Journal of Alloys and Compounds **275 –277**: 574 –577.

T. Goto, T. Kimura, G. Lawes, A. P. Ramirez, and Y. Tokura (2004). "Ferroelectricity and Giant Magnetocapacitance in Perovskite Rare-Earth Manganites." Phys. Rev. Lett. **92**(25): 257201.

T. Katsufuji, S. Mori, M. Masaki, Y. Moritomo, N. Yamamoto, and H. Takagi (2001). "Dielectric and magnetic anomalies and spin frustration in hexagonal $RMnO_3$ (R=Y, Yb, and Lu)." Phys. Rev. B **64**(10): 104419.

T. Kimura, T. Goto, H. Shintani, K. Ishizaka, T. Arima and Y. Tokura (2003). "Magnetic control of ferroelectric polarization." Nature **426**(6): 55.

T. Kimura, S. Kawamoto, I. Yamada, M. Azuma, M. Takano, and Y. Tokura (2003). "Magnetocapacitance effect in multiferroic $BiMnO_3$." Phys. Rev. B **67**(18): 180401.

T. Kimura, G. Lawes, A.P. Ramirez (2005). "Electric Polarization Rotation in a Hexaferrite with Long-Wavelength Magnetic Structures." Phys. Rev. Lett. **94**(13): 137201.

T. Portengen, Th. Ö streich, and L. J. Sham, (1996). "Theory of electronic ferroelectricity." Phys. Rev. B **54**(24): 17452.

T. Yoshimura, N. Fujimura, and T. Ito (1998). "Ferroelectric properties of c-oriented $YMnO_3$ films deposited on Si substrates." Appl. Phys. Lett. **73**(3): 414.

W. Eerenstein, F. D. Morrison, J. Dho, M. G. Blamire, J. F. Scott, and N. D. Mathur

(2005). "Comment on "Epitaxial $BiFeO_3$ Multiferroic Thin Film Heterostructures" " Science **307**: 1203a.

W. Eerenstein, N. D. Mathur & J. F. Scott, (2006). "Multiferroic and magnetoelectric materials." Nature **442**: 17.

W. Eerensteing, F. D. Morrison, J. F. Scott, and N. D. Mathur, (2005). "Growth of highly resistive $BiMnO_3$ films." Appl. Phys. Lett. **87**(10): 101906.

W. Prellier, Ph. Lecoeur, and B. Mercey, (2001). "Colossal-magnetoresistive manganite thin films." J. Phys.: Condens. Matter **13**(48): R915.

W. Prellier, M. P. Singh, and P. Murugavel, (2005). "The single-phase multiferroic oxides: from bulk to thin film." J. Phys.: Condens. Matter **17**: R803–R832.

WeidaWu, V. Kiryukhin, H.-J. Noh, K.-T. Ko, J.-H. Park, W. Ratcliff II, P. A. Sharma, N. Harrison, Y. J. Choi, Y. Horibe, S. Lee, S. Park, H. T. Yi, C. L. Zhang, and S.-W. Cheong (2008). "Formation of Pancakelike Ising Domains and Giant Magnetic Coercivity in Ferrimagnetic $LuFe_2O_4$." Phys. Rev. Lett **101**(13): 137203.

Y. L. Ma, Y. Liu, J. Li, ; H. L. Du, J. Gao, (2009). "Magnetic Anisotropy in $LuFe_2O_4$ Single Crystal." IEEE Transaction on magnetics **45**(6): 2608.

Y.N. Venevtsev, V.V. Gagulin (1994). "Search, design and investigation of seignettomagnetic oxides." Ferroelectrics **162**(1): 23-31.

Y. Zhang, H. X. Yang, C. Ma, H. F. Tian, and J. Q. Li (2007). "Charge-Stripe Order in the Electronic Ferroelectric $LuFe_2O_4$." Phys. Rev. Lett. **98**(24): 247602.

Y. Zhang, H. X. Yang, Y. Q. Guo, C. Ma, H. F. Tian, J. L. Luo, and J. Q. Li, (2007). "Structure, charge ordering and physical properties of $LuFe_2O_4$." Phys. Rev. B **76**(18): 184105.

Z. J. Huang, Y. Cao , Y. Sun, Y. Y. Xue, & C. W. Chu (1997). "Coupling between the ferroelectric and antiferromagnetic orders in $YMnO_3$." Phys. Rev. B **56**: 2623.